RÉPUBLIQUE ALGÉRIENNE DÉMOCRATIQUE ET POPULAIRE
MINISTÈRE DE L'ENSEIGNEMENT SUPÉRIEUR ET DE LA RECHERCHE SCIENTIFIQUE

ÉCOLE NATIONALE POLYTECHNIQUE

المدرسة الوطنية المتعددة التقنيات
Ecole Nationale Polytechnique

Département de Génie Mécanique

End of studies project thesis

Submitted in partial fulfillment of the requirements for the State Engineer Degree in Mechanical Engineering

---

Box-Behnken optimization of parameters influencing rotary friction welding joints

---

BOUTIARA Abdelhak

Under the supervision of
Dr. SAIDI Djamel and **Dr. JABBAR HASSAN Ammar**

Publicly presented and defended on the 2^{nd} of July, 2024

Jury members :

President	Dr. BELKACEMI Yacine	ENP
Supervisor	Dr. SAIDI Djamel	ENP
Co-supervisor	Dr. JABBAR HASSAN Ammar	USTHB
Examiner	Dr. SEDJAL Hamid	ENP

ENP 2024

RÉPUBLIQUE ALGÉRIENNE DÉMOCRATIQUE ET POPULAIRE
MINISTÈRE DE L'ENSEIGNEMENT SUPÉRIEUR ET DE LA RECHERCHE SCIENTIFIQUE

ÉCOLE NATIONALE POLYTECHNIQUE

المدرسة الوطنية المتعددة التقنيات
Ecole Nationale Polytechnique

Département de Génie Mécanique

End of studies project thesis

Submitted in partial fulfillment of the requirements for the State Engineer Degree in Mechanical Engineering

---

Box-Behnken optimization of parameters influencing rotary friction welding joints

---

BOUTIARA Abdelhak

Under the supervision of
Dr. SAIDI Djamel and **Dr. JABBAR HASSAN Ammar**

Publicly presented and defended on the 2^{nd} of July, 2024

Jury members :

President	Dr. BELKACEMI Yacine	ENP
Supervisor	Dr. SAIDI Djamel	ENP
Co-supervisor	Dr. JABBAR HASSAN Ammar	USTHB
Examiner	Dr. SEDJAL Hamid	ENP

ENP 2024

RÉPUBLIQUE ALGÉRIENNE DÉMOCRATIQUE ET POPULAIRE
MINISTÈRE DE L'ENSEIGNEMENT SUPÉRIEUR ET DE LA RECHERCHE SCIENTIFIQUE

ÉCOLE NATIONALE POLYTECHNIQUE

المدرسة الوطنية المتعددة التقنيات
Ecole Nationale Polytechnique

Département de Génie Mécanique

Mémoire de projet de fin d'études pour l'obtention du diplôme d'Ingénieur d'état en Génie Mécanique

---

Optimisation de Box-Benken des paramètres influents sur le cordon de soudure par friction rotative

---

BOUTIARA Abdelhak

Supervisé par
Dr. SAIDI Djamel et **Dr. JABBAR HASSAN Ammar**

Présenté et soutenu publiquement le 02 Juillet 2024

Membres du jury :

Président	Dr. BELKACEMI Yacine	ENP
Encadrant	Dr. SAIDI Djamel	ENP
Co-encadrant	Dr. JABBAR HASSAN Ammar	USTHB
Examinateur	Dr. SEDJAL Hamid	ENP

ENP 2024

ملخص

تركز هذه الأطروحة على تحسين العوامل المؤثرة على وصلات اللحام بالاحتكاك الدوراني (RFW) باستخدام تصميم التجارب بوكس-بنكن. يُعد اللحام بالاحتكاك الدوراني عملية لحام في الحالة الصلبة تنتج وصلات عالية الجودة بخصائص ميكانيكية فائقة، خاصةً بالنسبة للفولاذ المقاوم للصدأ AISI 304. تم دراسة عوامل مختلفة مثل سرعة الدوران وضغط الاحتكاك ووقت الاحتكاك. تشير النتائج إلى أن تصميم بوكس-بنكن فعال في استكشاف العلاقات بين هذه العوامل وتحسين عملية اللحام. توفر النتائج رؤى هامة لتحسين الخصائص الميكانيكية للفولاذ المقاوم للصدأ AISI 304.

الكلمات المفتاحية : التحسين، اللحام بالاحتكاك الدوراني، الفولاذ المقاوم للصدأ، تصميم التجارب، وصلات اللحام

Résumé

Cette thèse se concentre sur l'optimisation des paramètres influençant les cordons de soudure par friction rotative (RFW) à l'aide du plan d'expériences Box-Behnken. Le soudage par friction rotative est un procédé de soudage à l'état solide qui produit des joints de haute qualité avec des propriétés mécaniques supérieures, en particulier pour l'acier inoxydable AISI 304. Différents paramètres tels que la vitesse de rotation, la pression de friction et le temps de friction ont été étudiés. Les résultats indiquent que le plan de Box-Behnken est efficace pour explorer les relations entre ces paramètres et optimiser le processus de soudage. Les résultats fournissent des indications significatives sur l'amélioration des propriétés mécaniques de l'acier inoxydable AISI 304.

Mots clés : Optimisation, Soudage par friction rotative, Acier inoxydable, Plan d'expériences, Cordon de soudure

Abstract

This thesis focuses on the optimization of parameters influencing rotary friction welding (RFW) joints using the Box-Behnken experimental design. RFW is a solid-state welding process that produces high-quality joints with superior mechanical properties, especially for AISI 304 stainless steel. Various parameters such as rotational speed, friction pressure, and friction time were investigated. The findings indicate that the Box-Behnken design is effective in exploring the relationships between these parameters and optimizing the welding process. The results provide significant insights into improving the mechanical properties of AISI 304 stainless steel.

Keywords : Optimization, Rotary friction welding, Stainless steel, Design of experiments, Welding joint

Dedications

I dedicate this work

In the first place to my dear parents for their unwavering support throughout my entire educational journey.

To my brother whose mentorship always proved precious.

To my sister and beloved nephew Samy.

To Bouraoui Land friend group with whom I made very special and unforgettable memories during these past 5 years.

To Amine, Mahmoud, Rayan, Ouanis, Lylia and everyone who made my journey in Polytech memorable.

To Anis, Sara, and Rahyl who helped me immensely making this thesis.

To all those who have directly or indirectly contributed to the realization of this project.

Thank you sincerely to everyone.

Abdelhak

Acknowledgments

I would like to express my sincere gratitude to everyone who has supported me throughout my research and the writing of this thesis.

First and foremost, I am deeply grateful to my supervisors, Dr. SAIDI and Dr. JABBAR HASSAN, for their invaluable guidance and continuous support during my research. Their insightful feedback and advice have greatly improved the quality of my work.

I also extend my sincere thanks to Dr. BELKACEMI for accepting to be president of the jury and also Dr. SEDJAL for taking the time and effort in examining this thesis.

I would like to show my gratitude to the Zouyed laboratory, the Research Centre In Industrial Technologies (CRTI), as well as ACMP usinage de précision for their invaluable help and services in making the experimental part of this thesis attainable.

Finally, I would like to thank Anis Menzou for his precious counsel, irreplaceable support, as well as the highest form of selflessness. Without him this thesis would not have been possible.

Table of Contents

List of Figures

List of Tables

List of Acronyms

- **FW** : Friction Welding
- **RFW** : Rotary Friction Welding
- **LFW** : Linear Friction Welding
- **FSW** : Friction Stir Welding
- **AISI** : American Iron and Steel Institute
- **DoE** : Design of Experiments
- **RSM** : Response Surface Methodology
- **BB** : Box-Behnken
- **ANOVA** : Analysis of Variance
- **SS** : Sum of Squares
- **MS** : Mean Square
- **UTS** : Ultimate Tensile Strength
- **HAZ** : Heat Affected Zone

General introduction

In the rapidly evolving field of mechanical engineering, welding processes play a crucial role in manufacturing and construction. Among these processes, rotary friction welding (RFW) stands out due to its ability to produce high-quality joints with superior mechanical properties. This thesis focuses on the optimization of parameters influencing rotary friction welding joints, specifically using the Box-Behnken design approach.

Despite the widespread use of RFW, the optimization of its parameters remains a complex task due to the numerous variables involved and their interactions. Traditional trial-and-error methods are time-consuming and often do not yield the best results. Therefore, a systematic approach is necessary to identify the optimal conditions for the welding process. The Box-Behnken design, a response surface methodology, offers an efficient way to explore the relationships between multiple parameters and their effects on the response variable, ultimately leading to the optimization of the welding process.

This study employs a combination of experimental and statistical methods to achieve the research objectives. The experimental work involves the preparation of AISI 304 stainless steel specimens, the application of the RFW process under different conditions, and the subsequent testing of the welded joints for mechanical properties and microstructural analysis. The Box-Behnken design is used to systematically vary the welding parameters and develop a response surface model. Statistical tools such as analysis of variance are employed to interpret the data and identify the optimal welding conditions.

The findings of this research are expected to contribute significantly to the field of welding technology by providing a deeper understanding of the RFW process and its optimization. The optimized parameters can lead to improved joint quality, enhanced performance, and broader applications of RFW in various industries. Additionally, the use of the Box-Behnken design demonstrates a robust approach to process optimization that can be applied to other manufacturing processes.

This thesis is structured as follows:

- Chapter 1: Rotary Friction Welding Process – Provides a detailed overview of the RFW process, its principles, stages, and variations.
- Chapter 2: Generalities on AISI 304 Stainless Steel – Generalities on AISI 304 Stainless Steel – Discusses the properties of AISI 304 stainless steel and examines some of the literature on its welding.
- Chapter 3: Design of Experiments – Addresses the goal of design of experiments and the purpose of evaluation metrics in ANOVA.
- Chapter 4: Experimental Methods – Describes the experimental setup, materials used, and testing procedures.

- Chapter 5: Results and Interpretations – Presents the experimental results and statistical analysis, leading to the optimization of welding parameters.
- General conclusion – Summarizes the findings, discusses their implications, and suggests directions for future research.

By systematically addressing the optimization of RFW parameters, this thesis aims to advance the field of welding technology and provide practical solutions for industrial applications.

Chapter 1

Rotary friction welding process

1.1 Introduction

This chapter provides a comprehensive overview of the RFW process, including its origin, principle, stages and variations. It further delves into some applications of the process while emphasizing its advantages and limitations. By understanding the underlying mechanisms and parameters influencing RFW, this chapter sets the foundation for optimizing welding conditions to achieve superior welded joints quality.

1.2 Friction welding

Known since the end of the XIX century, but rarely used, friction welding developed in its industrial form in the Soviet Union around 1956, then in Great Britain and the United States a few years later. [1]

Friction Welding is a variation of pressure welding in which friction-induced heat helps the components to be welded to one another while forming the welded connection without melting the metal. Here, we produce a significant quantity of localized, intense heat creation, and deformation, which uses less energy and produces a very strong weld. Since the technique of solid state welding does not result in a molten pool, solidification mistakes are eliminated. With FW, two distinct materials with disparate mechanical and thermal characteristics can be joined without sacrificing the weld's strength. Because of its low cost, very precise operations, reproducibility, and reliability, FW is chosen over conventional techniques. Rotary friction welding being the most popular variant it can be classified into Direct Drive Friction welding and Inertial Drive Friction Welding. [2]

The definition of friction welding process in the American Welding Society (AWS) C6.1-89 Standard is as follows : 'Friction welding is a solid-state joining process that produces coalescence of materials under compressive force contact of workpieces rotating or moving relative to one another to produce heat and plastically displace material from the faying surfaces. Under normal conditions, the faying surfaces do not melt. Filler metal, flux, and shielding gas are not required with this process'. [3]

1.3 Types of friction welding

Due to the expansion of the welding field, and depending on how friction is produced, there are different forms and methods of applying friction welding, including :

- Rotary friction welding
- Linear friction welding
- Friction stir welding

1.3.1 Friction stir welding

The foundation of friction stir welding is the idea that friction between the tool and the components to be connected can be used to transform the mechanical energy generated by the tool's rotation and pressure into thermal energy. The basic idea is to press a rotating tool with a specific form between the ends of the parts that need to be connected. The material undergoes localized alterations due to the heat generated, which favor the formation of the joint by changing from a high-strength to a low-strength behavior. After that, joining is done without the use of filler metal and before the material reaches its melting point. [4]

Over the past two decade, FSW has been explored by many industries, including aerospace, automotive and marine one of the main reasons for it being its ability to assemble parts with widely differing cross-sections. [5]

1.3.2 Linear friction welding

When using linear friction welding (LFW), the components move in relation to one another when one is stationary and the other is in motion, all while under normal friction pressure, with a tiny linear displacement (amplitude) occurring in the plane of the joint to be formed. [3] Surface oxides and other impurities are eliminated, as is the plasticised material, allowing metal-to-metal contact between pieces and the formation of a junction. [6]

This process dates back to as early as 1929 [6] and is widely used to assemble blisks (blades and disks) for aircraft fan and compressor rotors to achieve weight reduction and performance improvement. [7]

1.3.3 Rotary friction welding

RFW is used to produce joints between two parts, at least one of which is rotationally symmetrical. It uses the thermal effect generated in the joint plane by the rapid rotation of the parts under pressure and friction. The heating power results from the resistive torque and the rotation speed, which is kept constant in principle. This is an all-round joining process, which is classified as a forging process. Due to material creep during friction and forging, the melting temperature is never reached.

This process is difficult to use on materials whose characteristics are not conducive to friction, particularly highly electrically conductive materials such as copper and its alloys. [1]

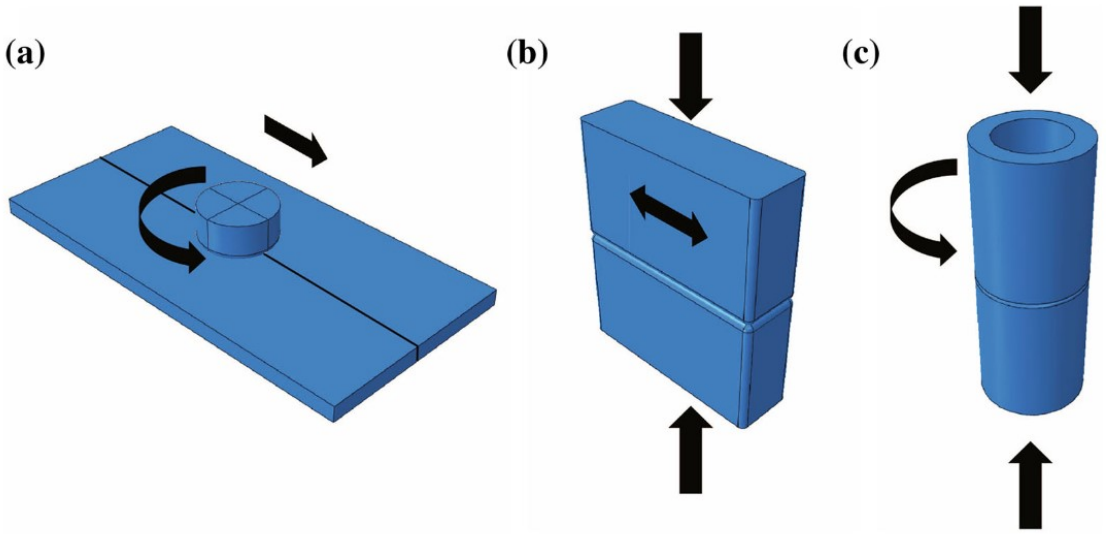

Figure 1.1: FSW, LFW and RFW processes[8]

1.4 Rotary friction welding principle

In this process, Friction is created almost exclusively by rotation. The rotating workpiece is clamped in a rotating chuck driven by a motor or flywheel, and must be rotationally symmetrical at least in the welding zone.

After contact, the surfaces heat up and become the source of heat which, through diffusion, raises the temperature of the part extremities. These become plastic and creep towards the periphery, forming a characteristic bead (Figure 1.2 C), while the heat continues to diffuse. When the welding temperature is reached, rotation is stopped and a forging force is applied to form the weld. [1]

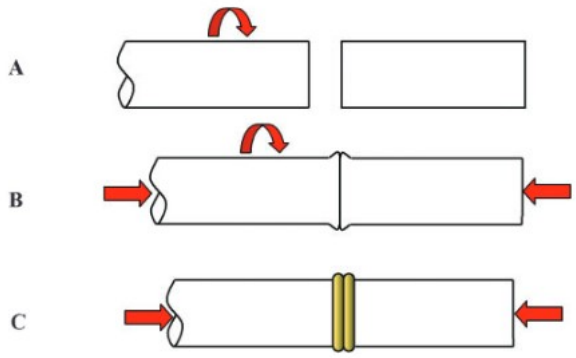

Figure 1.2: Basic steps in rotary friction welding process[3]

In practice, RFW is naturally applied to two cylindrical parts, plain or hollow, with the same cross-section at the joint. Applications are therefore mainly to be found in the construction of mechanical parts. [1]

A rotary friction welding operation is carried out on a highly specific machine (Figure 1.3), often adapted to a particular type of assembly. [1]

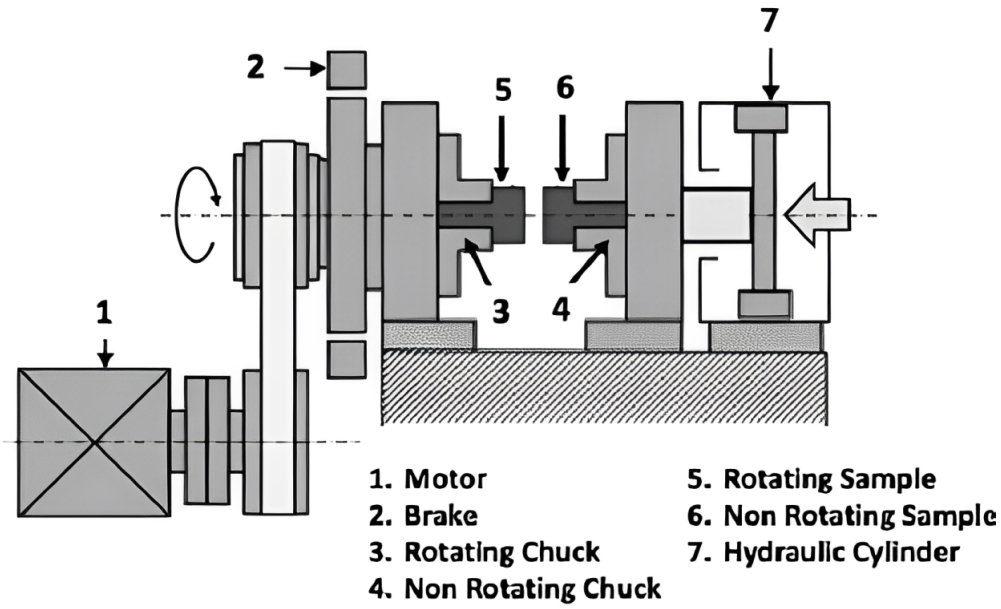

Figure 1.3: RFW machine [9]

Dissimilar materials that cannot be welded with other processes (TIG or GMAW) can be welded with the rotary friction process, such as aluminum or copper on steel [10], such as illustrated in Figure 1.4

Figure 1.4: Weldability of dissimilar materials using RFW [11]

1.5 Stages of rotary friction welding process

The rotary friction-welding mechanism essentially comprises two stages : the friction phase and the forging phase.

1.5.1 Friction phase

Figure 1.5 shows the variation in frictional torque over time during the friction phase. The variations in resistive (or frictional) torque divide the friction phase into four distinct stages: the stage of dry friction of the two previously prepared surfaces, the stage of transition or decrease in frictional torque, the stage of self-regulation and finally the stage of deceleration. [12]

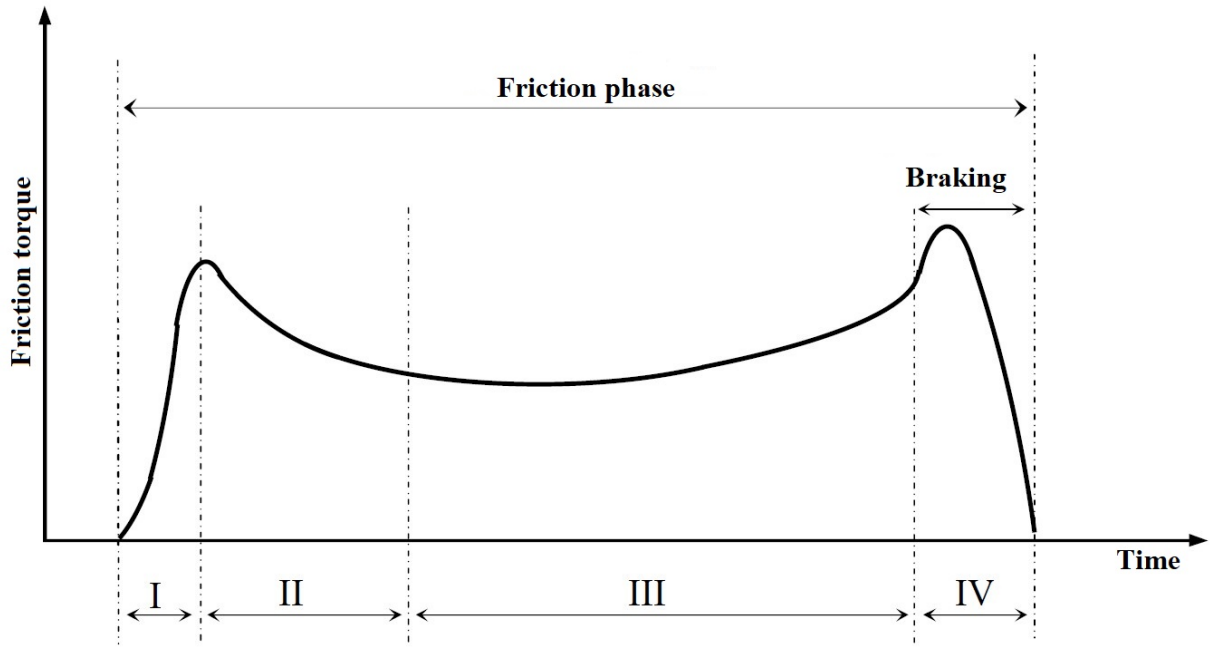

Figure 1.5: Variation of friction torque during the friction phase [12]

- Stage I : This stage begins when the two parts come into contact and start to rub against each other. It corresponds to the start of the welding cycle, during which dry friction occurs between the two surfaces.

  The asperities of the two surfaces seize up and tear each other off, as shown in Figure 1.6(a, b). The fragments torn off are more or less numerous and large, depending on the values of rotation speed and axial force. The debris digs wide furrows in the soft surface, leading to the destruction of the work-hardened layer (Figure 1.6c).

- Stage II : This stage is transient, starting when the torque begins to decrease after the initial maximum value, and ending when it reaches an almost constant equilibrium value. The plastic layer at the interface begins to be expelled towards the periphery under the effect of inertial (radial) and contact (normal) forces (Figure 1.6d). The expelled material begins to form a spiral (or bead) around the interface.

- Stage III : This is a stage of equilibrium or self-regulation of the friction torque. Moreover, the rate of axial shortening and the axial force remain constant during this period. The temperature of the interfacial layer heats the adjacent metal by conduction, leading to even material consumption over time.

- Stage IV : This is the deceleration stage, starting when braking is applied to stop the rotating part. During this stage, the plasticized layer moves towards the periphery of the parts, helping to increase the volume of the bead as the speed decreases.

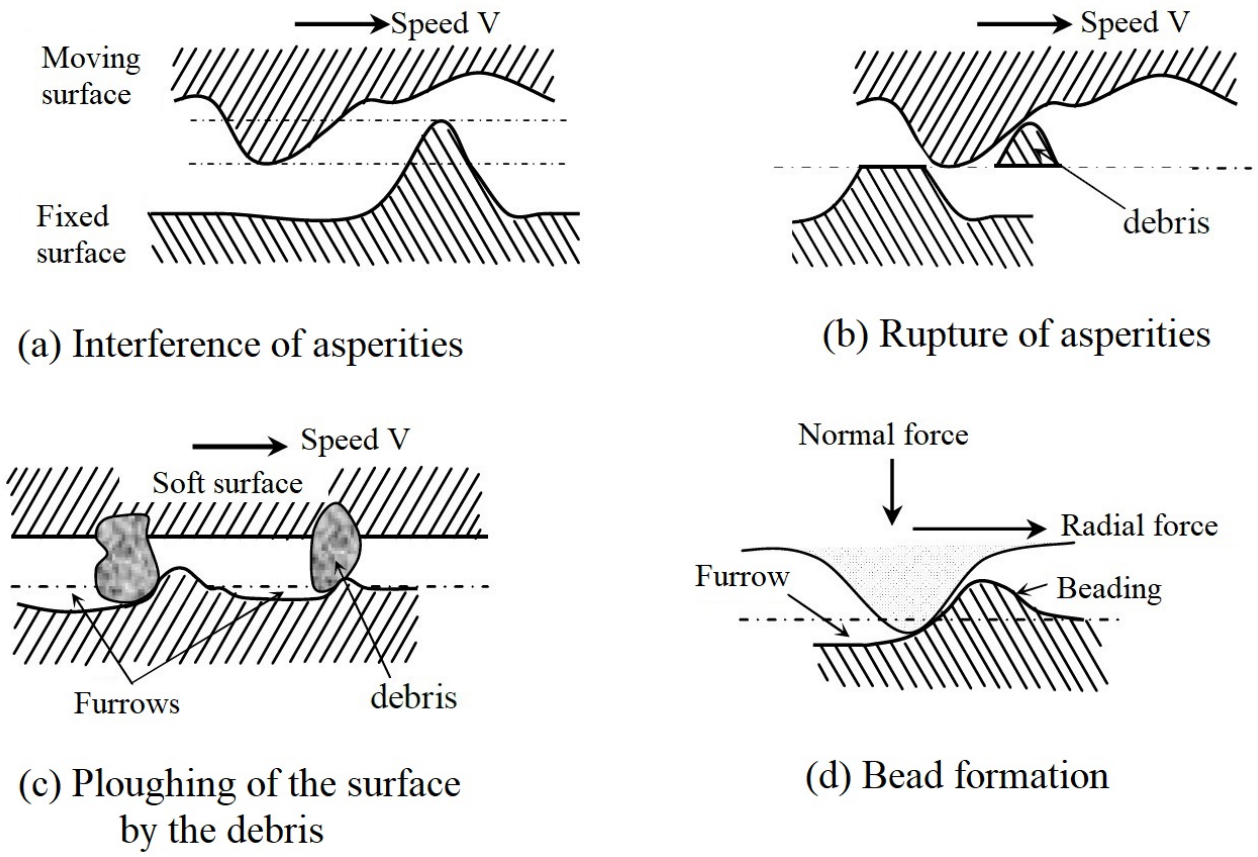

Figure 1.6: Surface interactions during friction phase [12]

1.5.2 Forging phase

Forging begins as soon as the rotating part stops. An axial force is maintained at a sufficient level to lead to hot forging of the interface material and its displacement (bead).

Forging force and duration have no connection with the friction phase. They depend solely on the metallurgical conditions of the materials to be welded.[12]

1.6 Rotary friction welding variations

There are two main process variations for rotary friction welding : direct drive (continuous drive) and inertia drive (stored energy). These differences depend on how kinetic energy is transformed into frictional heat.

1.6.1 Direct drive friction welding

1.6.1.1 Principle

One component is kept immobile during the continuous drive process while the other rotates at a constant speed. After that, the friction force is provided to cause the two parts to rub against

one another. The drive is released and a brake is applied to halt the spinning component when a predefined weld time or axial shortening is attained. Up until the weld has cooled, the axial force is either kept constant or increased. [3]

This particular variant of the process is the one that will be used in our work.

1.6.1.2 Parameters

The parameters required for direct-drive friction welding are as follows :

- Rotational speed
- Friction pressure (or friction force)
- Friction time
- Forge pressure (or forge force)
- Forge time

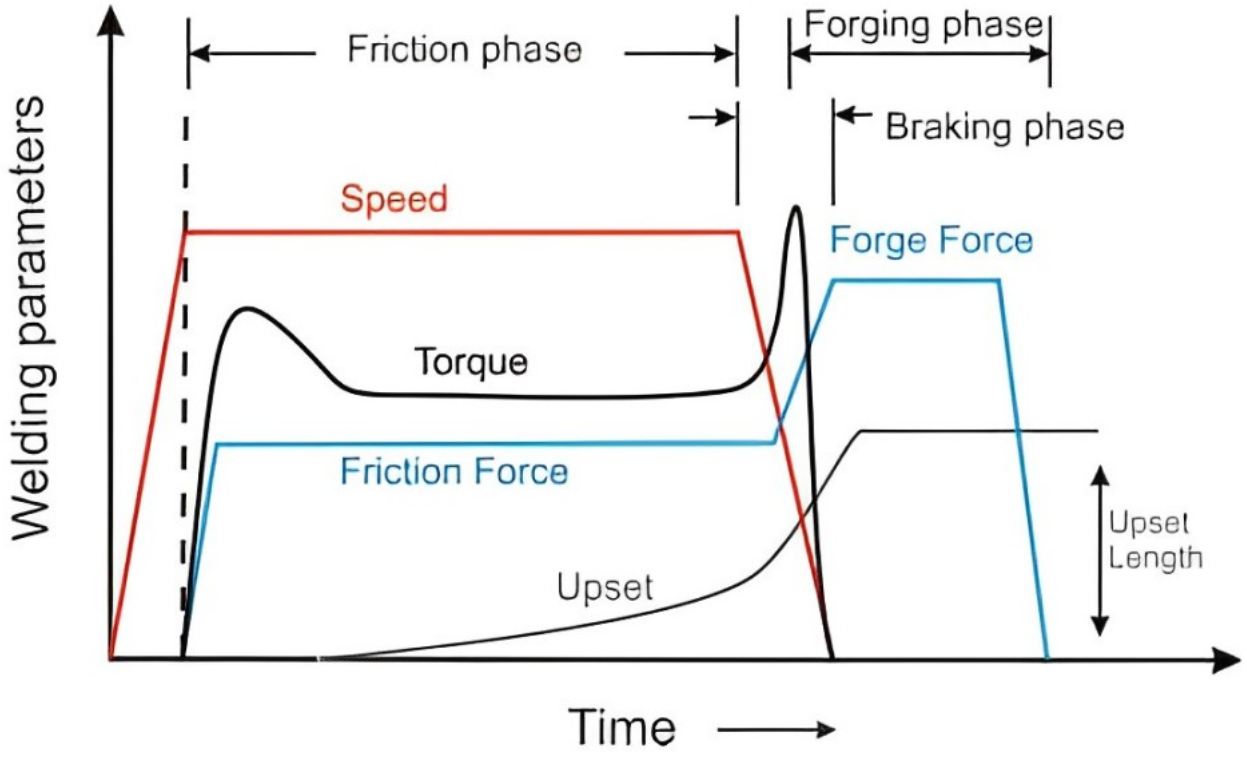

Figure 1.7: Evolution of welding parameters in direct drive process [3]

1.6.2 Inertia drive friction welding

1.6.2.1 Principle

One workpiece is kept immobile during the inertia process, and the other is fastened to a flywheel. By spinning the flywheel assembly to a specific speed, a predefined amount of energy is stored.

Next, an axial force is given and the drive to the flywheel assembly is disconnected, causing the two parts to rub against one another. At the rubbing interface, heat is produced using the flywheel's stored energy. The speed of rotation slows down as rubbing continues until the rotating component finally stops. Up until the weld has solidified, the axial force is maintained. During the welding cycle in this process, the rotational speed is continuously changing. [3]

1.6.2.2 Parameters

The parameters required for inertia friction welding are as follows :

- Flywheel mass (expressed by moment of inertia)
- Rotational speed
- Friction pressure (or friction force)
- Forge pressure (or forge force)

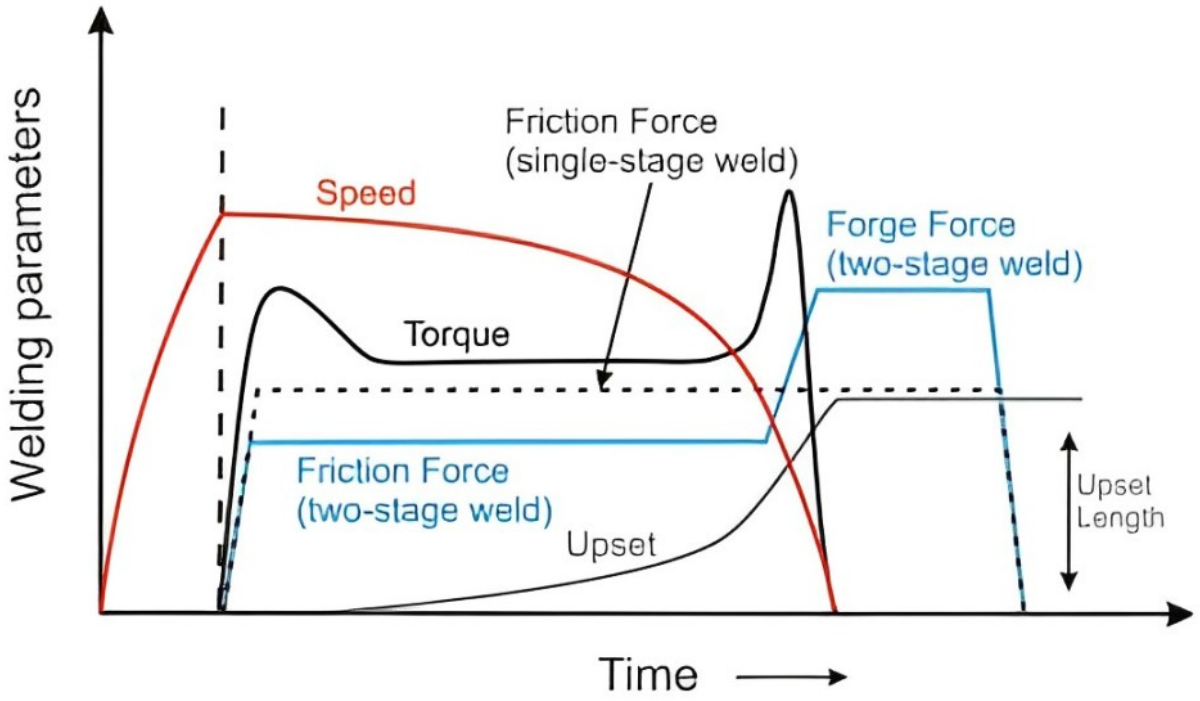

Figure 1.8: Evolution of welding parameters in inertia drive process [3]

1.7 Applications

Many different industries use the RFW process to join a wide range of components. These include sectors like oil and gas exploration, general mechanical engineering, electrical, aerospace, automotive, and construction machines. [11]

Technological trends like lightweight design and e-mobility place a high value on welding process expertise since it enables the low-cost industrial joining of various material combinations.

Figure 1.9 shows some of the uses of rotary friction welding in different applications.

Figure 1.9: Different applications of RFW [11]

Figure 1.9 (01) : Heat exchanger, Figure 1.9 (02) : Hollow valve, Figure 1.9 (03) : Wheel rim, Figure 1.9 (04) : Cardan shaft, Figure 1.9 (05) : Turbo loader, Figure 1.9 (06) : Hollow piston

1.8 Advantages and limitations

Rotary friction welding offers many advantages over other processes, but it also presents certain limitations that need to be taken into account.

1.8.1 Advantages

- High-quality assemblies with good metallurgical structure as the material is not melted.
- Parts with widely differing cross-sections can be joined, provided certain precautions are taken.
- Dissimilar materials can be joined, such as aluminum or copper to steel, which provides a large domain of applications.
- Excellent reproducibility and automation possibilities, which reduces human error.
- No need for highly qualified certified welders.
- No filler metals required in the process.
- Absence of shielding gases, flux and welding fumes which makes the process ecological.

1.8.2 Limitations

- Necessity of machining the beading after the process, therefore material consumption afterwards is needed.
- One of the parts to be welded must have an axis of symmetry so that it can be rotated around this axis.
- Certain materials, such as graphite, iron sulfide and lead, cannot be welded due to their low coefficients of friction.
- When welding very large sections, the machine's capacity can be a limiting factor.
- A high investment costs for equipment.

1.9 Conclusion

Rotary friction welding hasn't reached its peak in industrial integration because of the niche applications it currently covers, but its development can be very significant, particularly in the mass-production mechanical engineering industry, such as the automotive industry. The process is known for its productivity, reliability, integration into the production line and consistency, all of which encourage its development.

A better quantitative assessment of the influence of welding parameters on joint qualities will enable better control over welding outcomes. This in-depth knowledge of welding conditions will enable us to better adapt welding to the needs of the industry and users.

Chapter 2

Generalities on the AISI 304 stainless steel

2.1 Introduction

Stainless steels were first industrialized in the early 20^{th} century, at this time, it was discovered that steels can withstand corrosion better than regular carbon steels if they contain at least 12% more chromium by weight. The rate of surface dissolution was slowed down by the passive protective layer that formed spontaneously as a result of the addition of chromium.

As metallurgy developed, it was discovered that additional alloying of steels with elements like nickel, copper, titanium, aluminum, molybdenum, nitrogen and sulfur could selectively create other desirable properties. Stainless steels can be further divided into a number of categories, These consist of austenitic, ferritic, martensitic, precipitation hardenable and duplex. [13]

This chapter focuses on AISI 304 stainless steel, it begins with an overview and some properties of austenitic stainless steels and the 300 series grades. Afterwards, a comprehensive literature review on the welding of AISI 304 stainless steel is presented, summarizing key studies and findings that highlight the effectiveness of various welding techniques, with a particular emphasis on RFW.

2.2 Austenitic stainless steels

Austenitic stainless steel is the most commonly used type of all the stainless steels, it holds the largest share of all types of stainless steels in worldwide markets as shown in Table 2.1.

Austenitic stainless steel is an iron-chrome-nickel system. As the nickel atoms arrange themselves in the face-centered cubic structure over a significant temperature range, the substitution of iron atoms with nickel atoms makes the austenite phase stable at very low temperatures. [14]

Because of its stable austenitic microstructure, austenitic stainless steel has interesting traits such as good formability, weldability, ductility, excellent toughness even at cryogenic temperatures, and a non-magnetic characteristic. It is also the most corrosion resistant of all grades because of the high percentage of chromium and nickel content. As a result, austenitic stainless

steels have grown to be the most popular and widely used of all stainless steel types. [15]

Table 2.1: Worldwide market shares of stainless steels [15]

Stainless steel categories	Market share
Austenitic	72%
Ferritic	24%
Martensitic	2%
Precipitation hardening	1%
Duplex	1%

2.3 The 300 series grades

The 300 series is based on the classic 18% chromium, 8% nickel stainless steel. It is the most widely used grade all over the world and is well-known for its high toughness (impact strength) at both high and low temperature conditions.

The 300 series is further defined by the carbon content as 'L' (Low) grades, straight grades and 'H' (High) grades. The L grade contains less than 0.03% carbon and is intended for extra corrosion resistance, this grade is mostly used for welding. The straight grade contains $0.03 - 0.08\%$ carbon and the H grade contains anywhere from $0.04 - 0.10\%$ carbon. The high carbon content helps the material hold its strength at high temperatures and is therefore often used in high temperature applications.

From an application perspective, the 300 series grades are applicable to a wide range of industries, including developing nuclear plants, the food and dairy, beverage, aerospace, and chemical processing industries, as well as home appliances. This series is commercially available in around 34 grades namely 304, 304L, 316 and 316L. [15]

2.4 International standards designations of AISI 304

Table 2.2 provides a comparison of stainless steel designations as defined by various international standards. It highlights the equivalencies and differences among the norms to facilitate better understanding and selection of materials.

Table 2.2: AISI 304 designations across different standards [16]

Standard	AISI	UNS	EN	EN No	BS	JIS
Designation	304	S30400	X5CrNi18-10	1.4301	EN 58E	SUS 304

2.5 Literature review on welding of AISI 304

The amount of work carried out on the AISI 304 stainless steel year's wise from 1992 to 2011 is presented in Figure 2.1 and the amount of work carried out using various welding processes is shown in Figure 2.2.

It is clear that research on AISI 304 became more and more popular after 2004, and that friction welding represents the most used process to weld it.

Based on the research reports from different researchers, it can be determined that the majority of them focused on high Amperage welding because for high base metal thickness. For higher thicknesses, from different welding techniques, the friction welding process is determined to be the most effective due to its low working temperature, minimal defects, and ability to produce welded joints that have excellent metallurgical structure. When it comes to welding thin sheets, GTAW is the most cost-effective method, however, when quality is the primary consideration beam welding with a laser is the best option. [13]

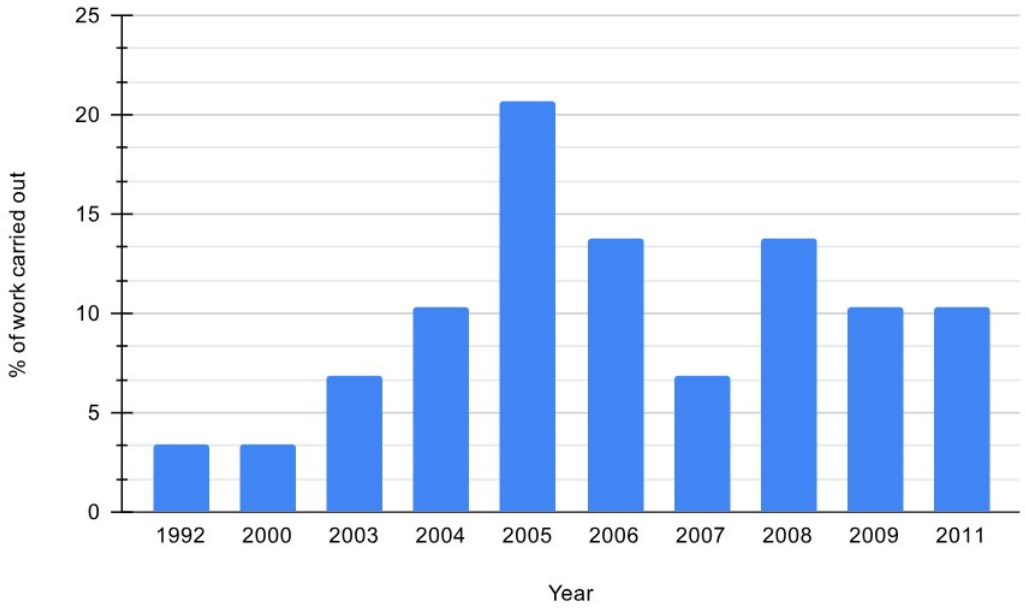

Figure 2.1: Percentage of work carried out year wise 1992-2011 [13]

When it comes to RFW, Handa et al. created an experimental setup for friction welded joints between austenitic stainless steel and low-alloy steel. The mechanical properties of friction welded AISI 304 with AISI 1021 steels were studied under different axial pressures. Welding samples were welded at a constant speed of 1250 rpm under varying axial pressures (75-135 MPa). The axial pressure has been found to be an influential parameter for the rotary friction welding process. [17]

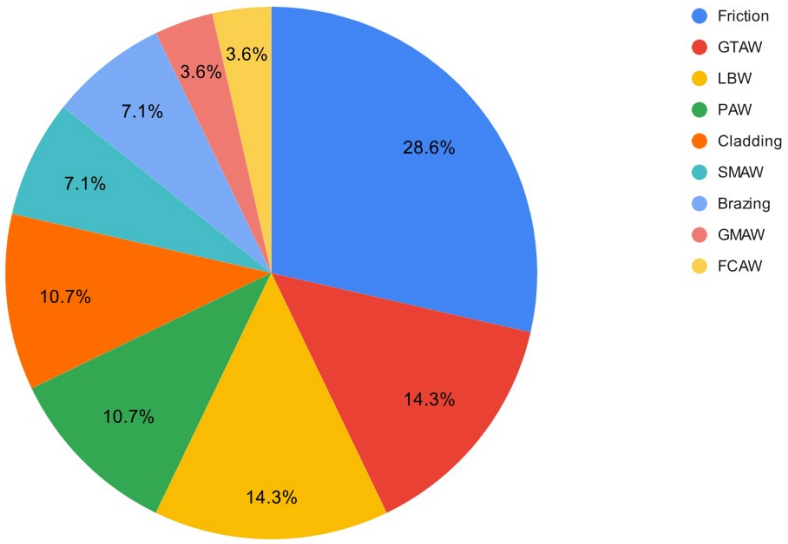

Figure 2.2: Contribution by various welding processes on the 304 1992–2011 [13]

Shubhavardhan et al. investigated solid state joining of dissimilar materials, AA6082 aluminum alloy and AISI 304 stainless steel, using a direct drive friction welding process. The tensile strength of the joints varied with increasing forging pressure and forging time, while friction pressure and friction time remained constant.
With the increase of forging pressure and forging time, the joint strength increased, and then gradually decreased after reaching a maximum value. Some of the welds had poor strength due to the accumulation of alloying elements at the joint interface due to long forging time.
The long forging time also resulted in the formation of an intermetallic reaction layer at the weld interface, which grew as the forging time increased. When the thickness of this layer exceeded a critical value, the joint became brittle and fractured at the weld interface. [17]

Alves et al. investigated the solid state joining of dissimilar materials AA1050 aluminum and AISI 304 stainless steel. These joints were created using a rotary friction welding process. Tensile tests and energy-dispersive X-ray spectroscopy were used to analyze the results.
The joint strength varied with increasing friction time and pressure. Joints were formed with superior mechanical properties than that of the AA1050 aluminum, with the fracture occurring away from the bonding interface.
The EDX analysis at the junction interface revealed interdiffusion between the main chemical components of the materials involved. [17]

Paventhan et al. investigated the optimization of friction welding parameters for dissimilar joints of AISI 304 austenitic stainless steel and commercial copper using a continuous drive friction welding machine. the varied parameters were friction and forging pressure as well as friction and forging time. Evaluation methods included tensile testing and microstructural analysis using scanning electron microscopy (SEM).
The study employed a central composite factorial design to develop empirical relationships for predicting tensile strengths. The optimal conditions identified were 60 MPA for both friction pressure and forging pressure, as well as 4 seconds for both friction and forging time, resulting in a maximum tensile strength of 489 MPa.
The microstructural investigation revealed the formation of hard zones and intermetallic com-

pounds at the interface, significantly influencing the joint properties. [18]

Jabbar Hassan et al. investigated the effect of friction time on the microstructure and mechanical properties of rotary friction welded similar material AISI 304-AISI 304 joints using a direct drive process. Various friction times were tested to analyze their influence on joint strength and material characteristics. The study employed tensile, compression, and micro-hardness tests.
Results indicated that increased friction time led to decreased mechanical properties as the ultimate tensile strength decreased from 718 MPa to 661 MPa and yield compression strength from 473 MPa to 452 MPa between 6.5 seconds and 10 seconds respectively. Tensile fractures occurred adjacent to the interface in the thermo-mechanical deformation zone (TMDZ) on the rotating side for all specimens, with reduced micro-hardness in that region.
The study concluded that longer friction times result in higher levels of micro-hardness at the welding interface due to dynamic recrystallization effects. The micro-hardness was highest at the weld interface and attenuated towards the TMDZ in the rotating side, influenced by heat distribution and mechanical deformation during the welding process. [19]

2.6 Conclusion

Rotary friction welding of AISI 304 stainless steel has been extensively studied in various contexts. Research has shown that optimizing process parameters such as rotational speed, friction time, and friction pressure significantly impacts the mechanical properties and bonding strength of the welded joints.

These studies collectively contribute to a comprehensive understanding of the friction welding process for AISI 304 stainless steel, highlighting its potential for producing almost defect-free joints with superior mechanical properties and corrosion resistance.

Chapter 3

Design of experiments

"**The proper method for inquiring after the properties of things is to deduce them from experiments**" [20]

Isaac Newton

3.1 Introduction

The experimenter, whatever his or her field of study, is always faced with the difficult problem of how to best organize his tests and how to obtain the right information in the shortest possible time and at the lowest possible cost. This is the question we shall endeavor to answer in this chapter.

A set of statistical methods for process improvement and planning are included in the Design of Experiments. With the use of DoE, the experimenter can modify the ideal parameter values to produce the best results and a resilient process—that is, one with the least amount of fluctuation. [21]

Scientists have only been tackling this subject for a short time. The first to tackle the problem were agronomists and statisticians. The techniques and concepts they developed are so general that they can be used in all fields. This science of test organization is relatively recent, starting with the work of Sir R.A. Fisher (early XX century). [22]

3.2 Goal of design of experiments

Experiments are typically performed to examine the way systems and processes behave. We can usually visualize a process as a combination of operations, machines, methods, people, and other resources that transforms some input (often a material) into an output that has one or more observable response variables.

Some of the process variables and material properties are controllable, whereas other variables are uncontrollable as shown in Figure 3.1. [23]

Design of experiments is the best way to organize these experiments that accompany scientific research or industrial studies. They are applicable to a wide range of disciplines and industries,

from the moment we investigate the relationship between a quantity of interest y, and variables x_i. Experimental designs use experimental data to describe the behavior of a quantity of interest in the form of a mathematical function that depends on the factors chosen. The function is of type:

$$y = f(x_1, x_2, ..., x_n)$$

where :

- y is the quantity in which the experimenter is interested, this quantity is called the response, output or the quantity of interest.
- x_i are variables on which the experimenter can act, these variables can be continuous or discontinuous; they are called factors. DoE enables us to study the the influence of a large number of factors without excessively multiplying the number of trials.
- f is mathematical function that best explains variations to the response y according to the different values given to the factors x_i. In the case of DoE, this mathematical function is often a polynomial. [22]

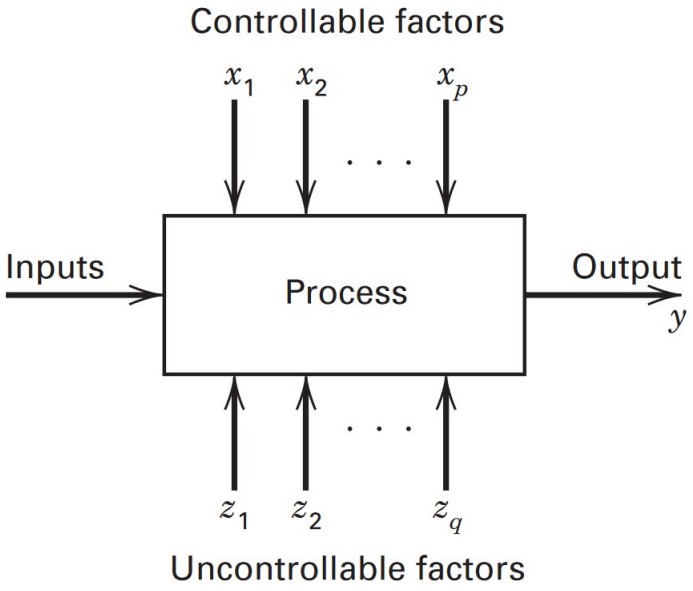

Figure 3.1: General model of a process or system [23]

3.3 Terminology

3.3.1 Experimental Space

The experimental space is composed of all the points of the plane factor 1 × factor 2 where each point represents an experimental trial.

If a third factor exists, it is also shown by a graduated, directed axis that is oriented perpendicular to the other two. The same technique holds for four elements or more, but in that case, geometric representation of the space is not possible. A pure mathematical representation of the experimental space (a four-dimensional hypercube) is then required. [24]

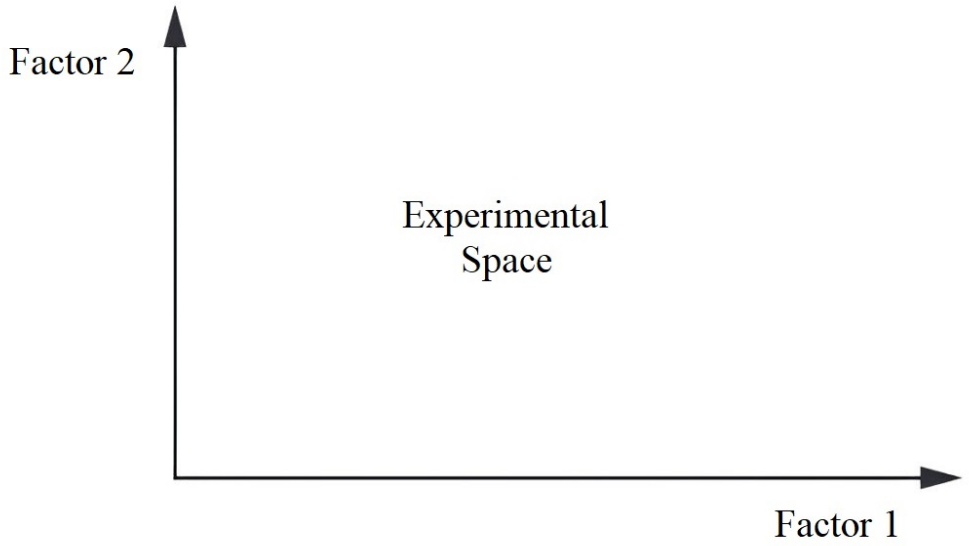

Figure 3.2: Experimental space of 2 factors [24]

3.3.2 Factor Domain

In general, we limit the variation of a factor under study to fall between two limits. These two bounds are defined by the experimenter based on the particulars of the study. The lower limit is called the low level and the upper limit is called the high level. The factor's domain of variation, or just the factor's domain, is the set that includes all possible values for a factor between the low and high levels.

To represent all factors in the same way, we indicate the high level by +1 and the low level by -1. Depending on the degree of the model, we choose the number of levels in the domain of a factor, i.e. two levels for a linear model and three levels for a second-degree model.[24]

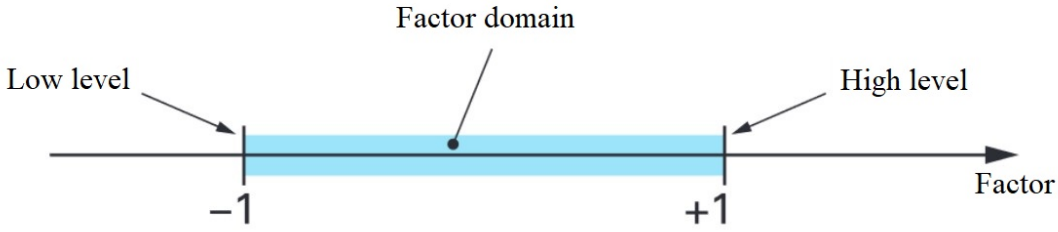

Figure 3.3: Domain of a factor [25]

3.3.3 Study Domain

In reality, the study is conducted in a specific area of the experimental space selected by the experimenter.

The levels of all factors and the constraints between them define the study domain. If there are no constraints, the study domain is represented by all points whose factor values lie between the low and high levels.[24]

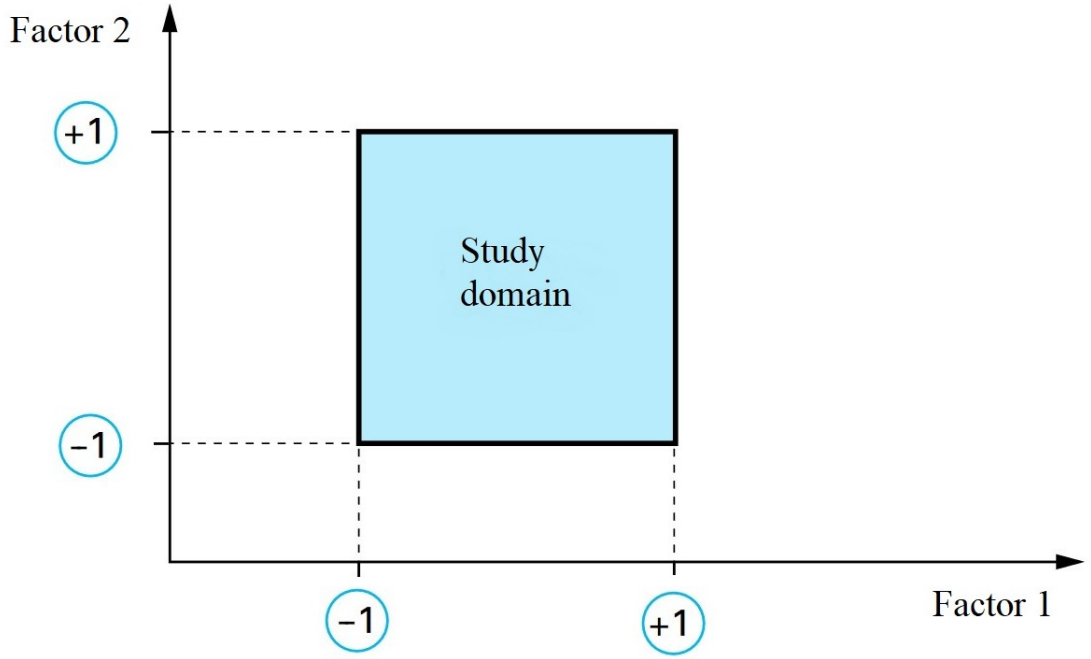

Figure 3.4: A full study domain [22]

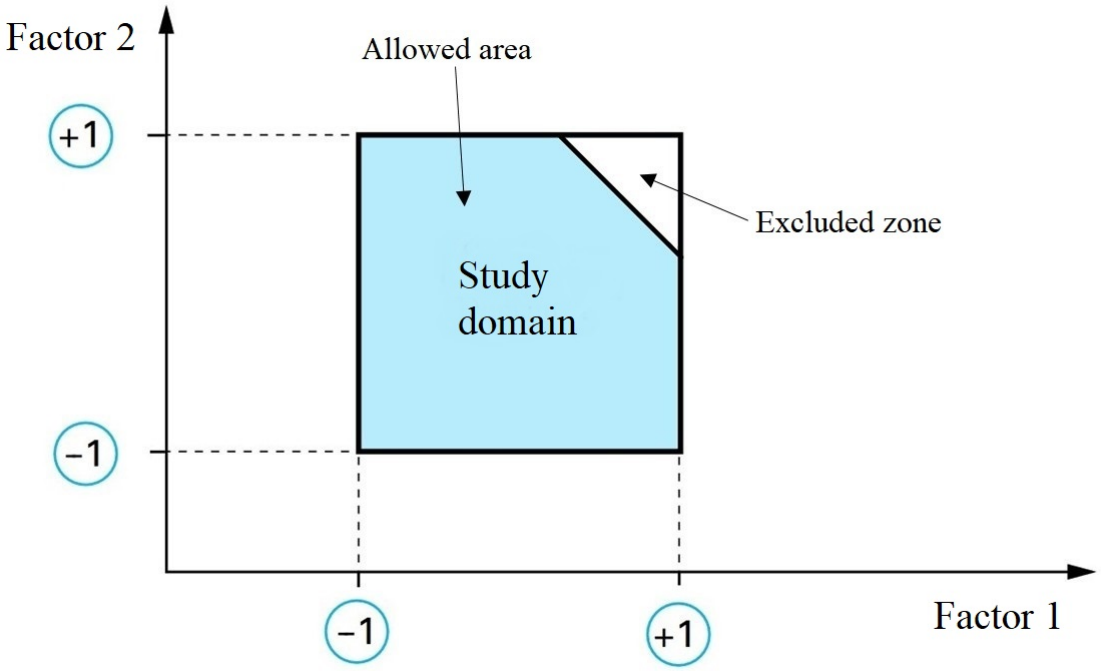

Figure 3.5: Study domain with a constraint between the factors [22]

3.3.4 Centered and scaled variables

Two significant changes happen when a factor's upper level is represented by +1 and its lower level by -1 : the center of the measurements moves and the measurement unit changes. These two changes involve the introduction of new variables called centered and scaled variables or also commonly called coded variables or coded units.

The conversion of the original variables A to the coded variables x (and vice versa) is given by the following equation, where A_0 is the central value in the original units. [24]

$$x = \frac{A - A_0}{Step} \tag{3.1}$$

Coded units have the advantage of being able to display designed experiments uniformly, irrespective of the parameters and study domains selected, making DoE quite generalizable.

3.4 General steps for conducting DoE

The general practical steps and guidelines for planning and conducting DoE are as follows [26]:

1. **Stating the objective :** Which includes clearly listing the problem that is going to be investigated in the experiment.
2. **Defining the response variable(s) :** Which is the experiment's measurable outcome, and it is based on the predetermined objectives.
3. **Selecting factors and levels :** Choosing the independent variables (factors) that can influence the response variable's change.
4. **Selecting a design type :** Choosing the right design type that suits the objective of the study and the constraints of experimenting if present.
5. **Performing the experiments :** Using the factor levels and running order provided by the design matrix.
6. **Data analysis :** Applying statistical methods such as regression and ANOVA, typically using some computer statistics software.
7. **Conclusion :** Interpreting the data, including graphical representations and validation of the results, ending with some practical recommendations.

3.5 Types of experimental designs

3.5.1 Screening designs

Their goal is to determine which of the main factors are significant and, in some cases, which second-order interactions come into play. This is the reason that these designs are often called

screening designs. These designs let us determine which of a large number of factors are influential. This is often the single goal of these experiments, so they are not often carried through to the stage of mathematical modeling and coefficient interpretation. Therefore, the mathematical models used are themselves far simpler.

The most common models are those having only main effects (first-degree terms) or models with main effects and second order interactions, depending on the objectives of the study. [24]

3.5.2 Response surface designs

Also called modeling designs, response surface designs are a collection of statistical and mathematical methods, they are used to create empirical mathematical models. Using these models can help achieve goals like prediction and optimization of single or multiple responses.

The postulated mathematical model used with response surface designs is a second-degree model with second-order interactions.

3.5.3 Mixture designs

Every factor is independent in traditional non-mixture designs, such as response surface and factorial designs. This implies that a factor's level can be freely selected, independent of the levels of the other components. Since the elements in mixture designs are the constituent quantities of a mixture, this freedom does not apply. The final component percent is determined by adding the total of the previous components because these ratios must always add up to 100%. [24]

As an example, if we want to optimize steel's tensile strength, we can vary the proportions of iron, carbon, copper, nickel and chrome in the alloy. But since the percentages of these constituents must add up to 100%, means it is impossible to use the other experimental designs.

3.6 Response surface methodology

Response surface methodology, or RSM, is a set of statistical and mathematical techniques that are helpful for modeling and analyzing situations where the goal is to optimize a response of interest that is influenced by multiple variables, whether the goal is to find a maximum, minimum or saddle point.

3.6.1 Numerical approach

The nature of the relationship between the response and the independent variables is unknown in most RSM problems. Finding a good approximation of the actual functional relationship between y and the set of independent variables is therefore the first step in the RSM model, also, the choice of the number and location of experimental points plays a pivotal role in DoE since we are looking for the minimum number of experiments while maintaining the best possible precision on the response surface. [23]

Usually, a low-order polynomial is used in a particular region of the independent variables. If the response is well modeled by a linear function of the independent variables, then the approximating function is the following first-order model :

$$y = \beta_0 + \beta_1 x_1 + \beta_2 x_2 + ... + \beta_n x_n + \varepsilon \tag{3.2}$$

If there is curvature in the system, then a polynomial of a higher degree must be used, such as the following second-order model :

$$y = \beta_0 + \sum_{i=1}^{n} \beta_i x_i + \sum_{i=1}^{n} \beta_{ii} x_i^2 + \sum_{i=1}^{n-1} \sum_{j=i+1}^{n} \beta_{ij} x_i x_j + \varepsilon \tag{3.3}$$

These systems can be written in a simpler way using matrix notation as follows :

$$\mathbf{y} = \mathbf{a}\, X + \mathbf{e} \tag{3.4}$$

Where :

- $\mathbf{y}$ is the response vector
- X is the design matrix which depends on the experimental points used in the design
- $\mathbf{a}$ is the coefficient matrix
- $\mathbf{e}$ is the error vector

This system of equations cannot be, in most cases, solved simply because there are fewer equations than there are unknowns. To solve the system we use linear regression based on the least squares. the results are estimations of the coefficients, denoted $\hat{\mathbf{a}}$. [24]

The results can be given as :

$$\hat{\mathbf{a}} = (X^t X)^{-1} X^t \mathbf{y} \tag{3.5}$$

with X^t being the transpose of X and $(X^t X)^{-1}$ the inverse of $X^t X$.

3.6.2 Graphical approach

Some of the most important tools of response surface methodology are the contour plots (Figure 3.6a) and the response surface plot (Figure 3.6b), which usually allow for a rather accurate graphical localization of factor settings that will result in an optimum response, be it minimizing or maximizing some effect or having it right on some target value.

These plots prove especially useful if there are no more than three influential variables. However, interpreting these plots becomes difficult when more variables are involved, necessitating a more thorough analysis.

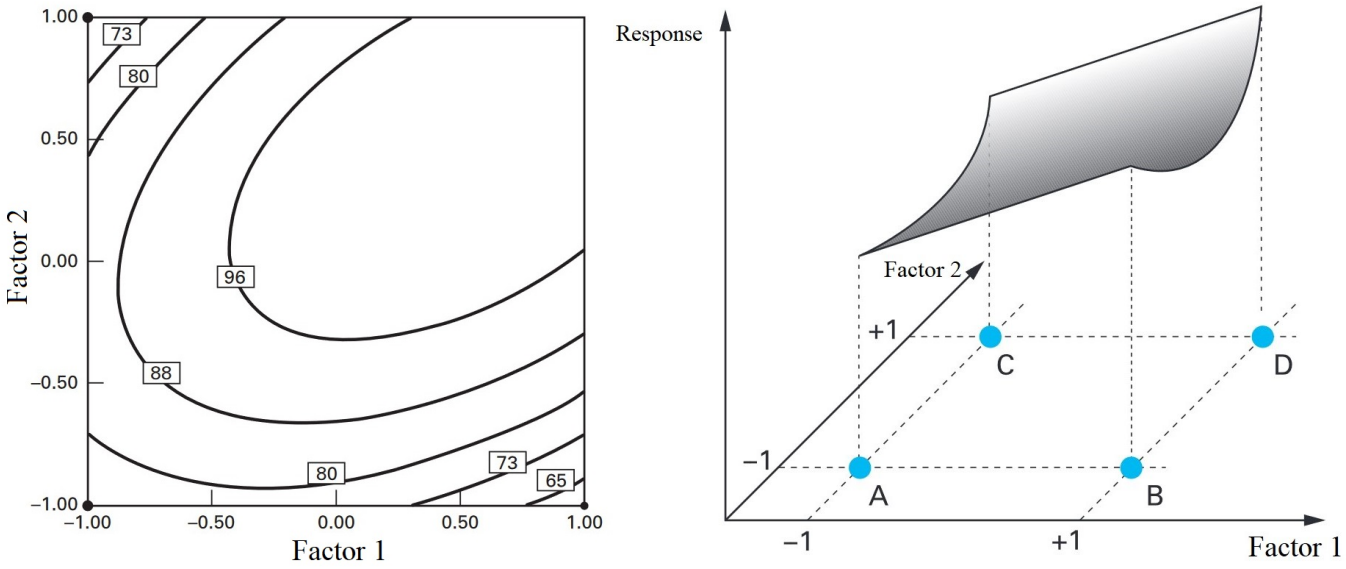

(a) Contour plot of 2 factors [23]

(b) Surface response of 2 factors [25]

Figure 3.6: Types of graphical representations of responses

3.6.3 Commonly used response surface designs

1. **Box-Behnken design**

   Box-Behnken designs enable second-degree models to be established directly with all factors having three levels. These designs have the sequentiality property and are simple to implement. Studying k factors allows one to keep the option to include new ones without losing the results of previously conducted tests. [24]

2. **Central composite design**

   The advantage of central composite designs lies in the fact that they easily follow on from a first factorial design (whether full or fractional) whose results cannot be explained by a first-degree model. The procedure is to run experiments corresponding to extra points called star points and center points and then perform the calculations on all the experiments as a whole. In this design each factor has five levels. For face-centered designs (where the star points are at the center of each face of the design space), there are only three levels per factor.

   Central composite designs are ideally suited for progressive acquisition of results. [22]

3.7 The Box-Behnken design choice

3.7.1 Overview

Box and Behnken's (1960) three-factor design is the most widely used method for estimating second-order models. It is usually made up of the three centerpoint runs and the twelve

midpoints of a cube's edges as shown in Figure 3.7. Compared to a central composite design (with the same number of centerpoint replicates), this design requires two fewer runs.

This and other Box-Behnken designs have the consistent advantage of requiring only three levels for each factor (-1, 0, and +1), as opposed to central composite designs with $\alpha \neq 1$, which require five levels. [27]

These designs are easy to implement and have the property of sequentiality, which means The first k factors can be studied, with the possibility of adding new ones without losing the results of tests already carried out. [24]

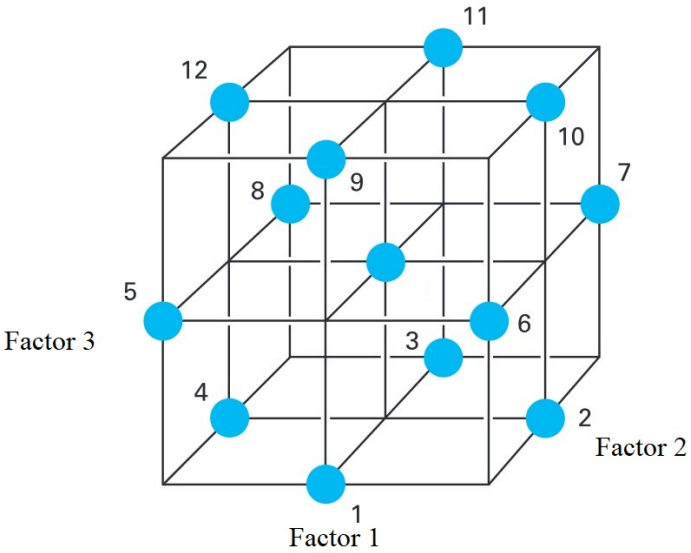

Figure 3.7: Box-Behnken cube for 3 factors [25]

3.7.2 Properties

- Very efficient in terms of the number of required runs.
- The design only requires 3 levels for each factor : -1, 0 and +1.
- BB design has the property of sequentiality (the possibility of adding new factors).
- There are no points at the cube's vertices. This can be useful when the corner points represent factor-level combinations that are difficult to test due to physical constraints.
- Prediction errors on calculated responses are smaller than experimental errors.

3.7.3 Box-Behnken design for 3 factors

Table 3.1 shows the different levels factors take in a 3 factor Box-Behnken design with 3 centerpoints.

Table 3.1: Three factor Box–Behnken design matrix [27]

Run	Factor 1	Factor 2	Factor 3
1	-1	-1	0
2	1	-1	0
3	-1	1	0
4	1	1	0
5	0	0	0
6	-1	0	-1
7	1	0	-1
8	-1	0	1
9	1	0	1
10	0	0	0
11	0	-1	-1
12	0	1	-1
13	0	-1	1
14	0	1	1
15	0	0	0

3.8 Analysis of variance

3.8.1 Definition

Analysis of variance is a statistical tool used to detect differences between experimental group means. If a difference between means is statistically significant, the difference is expected (with a certain probability) to reappear if the study is replicated. A non significant difference implies that you cannot rule out the possibility that the mean differences that do exist in the sample data occurred by chance. [28]

ANOVA is recommended in experimental designs with one dependent variable that is a continuous parametric numerical outcome measure, and multiple experimental levels within one (One-way ANOVA) or more (Two-way ANOVA) independent variables. [29]

The development of ANOVA for the purpose of analyzing agricultural experiment results was initiated by Sir Ronald Fisher. Nowadays, almost all statistical packages come with ANOVA, so researchers in all experimental sciences can use it. [30]

3.8.2 Assumptions of ANOVA

Certain assumptions are made about the nature of the data when tests are devised.
The underlying mathematics of general linear models is covered by the assumptions for ANOVA. A data set must specifically satisfy the following requirements in order to be used for ANOVA:

1. **Independence :** The value of each observation for each subject is generally assumed to be independent of (i.e., unrelated to, or unaffected by) the value of any other observation in parametric analysis. [29]

2. **Normality :** We assume a normal, or gaussian, probability distribution for the random errors within each level and the deviations from each group mean. [30]

3. **Homogeneity of variance :** The amount of data dispersion must be similar across all levels since it is assumed that the variance within each design level is a distinct estimate of the same population variance. [28]

3.8.3 Metrics used

1. **Coefficient of determination R^2**

   R^2 serves as a useful tool for evaluating the quality of a linear model.

   This statistic is defined as the ratio of the sum of squares of the predicted responses corrected for the mean, to the sum of squares of the observed responses (also corrected for the mean). [24]

$$R^2 = \frac{SS_R}{SS_T} = \frac{\sum_{i=1}^{n}(f_i - \bar{y})^2}{\sum_{i=1}^{n}(y_i - \bar{y})^2} \tag{3.6}$$

   If the residuals are zero, R^2 is equal to 1, regardless of the quality of the model.

2. **Adjusted coefficient of determination R^2_{adj}**

   Since R^2 always increases as we add terms to the model, some regression model builders prefer to use an **adjusted** R^2 statistic defined as

$$R^2_{adj} = 1 - (1 - R^2)\,\frac{n-1}{n-p-1} \tag{3.7}$$

   Where p is the number of independent variables in the model, and n is the sample size.

   As variables are added to the model, the R^2_{adj} statistic generally does not increase, In fact, the value of it will frequently decrease if unnecessary terms are added. [23]

3. **F - Statistic**

   The F-statistic (in honor of Sir Fisher) is the ratio of between group variance to within group variance.

$$F = \frac{MS_b}{MS_w} \tag{3.8}$$

   The F-statistic is used to test the null hypothesis (the hypothesis that there is no difference between means and that the independent variables had no effect on the response). [28]

   Large values of the F-statistic provide evidence against the null hypothesis, and thus, it shows that the independent variables have a significant effect on the response. [30]

4. **t - value**

   The t-ratio tells us specifically how far a sample mean deviates from the population mean in units of an estimated standard errors of the mean. [31]

$$t = \frac{M - \mu}{SE_M} \tag{3.9}$$

   The t-test is a test of a hypothesis about a population mean μ when the population standard deviation σ is not known. This test is used when researchers want to know if a sample is representative of a population and/or if a particular variable has a significant effect. [32]

5. **p - value**

   The p-value is generated by the t-test statistic, it measures the probability that an event is rare. The Null hypothesis is rejected when the p-value yielded by the t-test is less than α which is the predetermined upper limit (By convention, α is typically set to 0.05). [29]

   It is not always easy to compute the exact p-value for a test. However, most modern computer programs for statistical analysis can report p-values. [23]

3.9 Minitab statistical software

Minitab is a data analysis software package designed for data analysis. It is widely used in a number of fields, including healthcare, manufacturing, and education. Minitab provides users with tools for statistical analysis, such as hypothesis testing, regression analysis, and ANOVA. Minitab also includes a variety of graphical tools to help users visualize data.

Minitab offers users tools for statistical analysis, six sigma quality improvement, and design of experiments, with the goals of product quality improvement and process optimization taken into consideration.

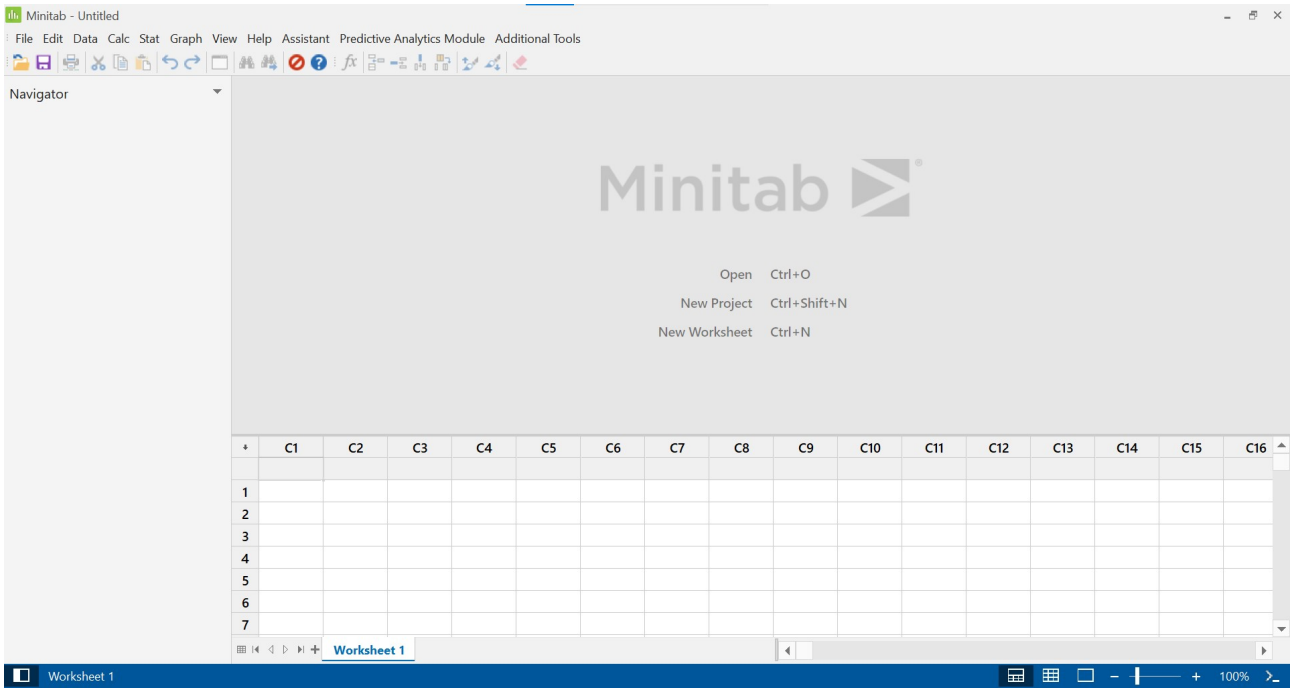

Figure 3.8: Minitab 21 graphical user interface

3.10 Conclusion

Using a variety of statistical tools and tests, the design of experiments approach consists of arranging the experimental strategy and analysis. By using experimental design, a strategy is established that yields results with the highest level of precision and the least variability by doing the fewest number of experiments possible.

Even though the DoE tool is not a new technique, its application has expanded rapidly in scientific areas over the past two decades, including in product quality improvement and process optimization. This rapid increase in its use is mostly due to the recent development of user-friendly statistical software packages.

The trend of DoE is still growing, and it is expected to continue to do so in the near future.

Chapter 4

Experimental methods

4.1 Introduction

This chapter outlines the experimental methods employed in this study to investigate the properties and performance of rotary friction welded joints of AISI 304 stainless steel. The focus is on the comprehensive examination of the materials used, the welding procedures, mechanical testing, and metallographic analysis. Each section details the methodologies applied to ensure rigorous and reproducible results, providing a clear understanding of the experimental framework supporting the findings presented in the following chapter.

4.2 Material used

4.2.1 Workpieces preparation

The AISI 304 stainless steel for this work was obtained as a round plain bar, measuring 12mm in diameter and 3000mm in length, with a weight of 2.7kg. This bar was then cut using a lathe machine into segments of 50mm (Figure 4.1a) to be later welded, and segments of 100mm (Figure 4.1b) to represent the base metal for later comparison purposes.

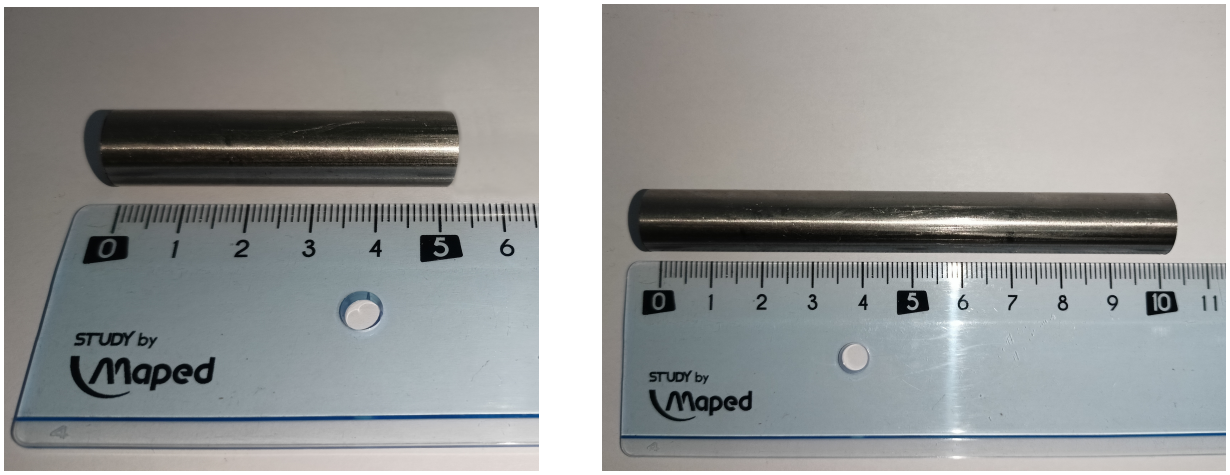

(a) The 50 mm workpiece (b) The 100 mm workpiece

Figure 4.1: The final workpieces after cutting

4.2.2 Chemical analysis

We used spectroscopy at Zouyed Laboratories in order to determine the exact chemical composition of our AISI 304. A sample of the stainless steel was prepared by mounting it in a thermosetting resin (Figure 4.1) and then the surface was polished to obtain a smooth, clean area for analysis. The analysis confirmed the presence of key elements, including iron, chromium, and nickel as well as other elements, which is consistent with the known composition of AISI 304 stainless steel. This non-destructive technique provided rapid and reliable results shown in Table 4.1, which are essential for the accurate characterization of the base material.

Figure 4.2: Spectroscopy sample mounted in a thermosetting resin

Table 4.1: Chemical composition of the base metal

Element	C	Cr	Ni	Al	Cu	Si	Mn	P	S	N	Mo	Fe
wt%	0.054	18.55	7.74	0.039	0.51	0.409	1.03	0.015	0.017	0.129	0.328	Bal

4.2.3 Mechanical and physical properties

Table 4.2 details the mechanical and physical properties of the base metal, providing a comprehensive analysis of its behavior and characteristics under various conditions. This information is crucial for understanding the material's performance and suitability for specific engineering applications.

These properties were obtained from tests conducted at the National Polytechnic School and the Research Center in Industrial Technologies (CRTI), and from the work of Jabbar Hassan et al. [33]

Table 4.2: Mechanical and physical properties of the base metal

Property	Value
Density	$8000\,Kg/m^3$
Ultimate tensile strength	736 MPa
Yield strength 0.2%	603 MPa
Modulus of Elasticity	193 GPa
Elongation	46%
Vickers hardness	263 HV

4.3 Welding conditions

4.3.1 The RFW machine used

The welding procedure was conducted at the Laboratory of Advanced Mechanics at Houari Boumediene University of Science and Technology (USTHB). The process utilized a direct drive RFW machine, developed as part of Dr Jabbar Hassan's PhD thesis.

The machine comprises several key components (Figure 4.3): the hydraulic system, which applies axial pressure; the asynchronous motor, which drives the rotation; the brakes, which provide instantaneous stopping of rotation; the chucks, which hold and secure the workpieces; and the programmable logic controller (PLC), which oversees and controls all these components.

Welding parameters are controlled by a numerical control system, making it easy to keep the welding operation under control. The RFW machine used can produce a maximum pressure of 300 MPa, enabling it to weld cylindrical parts up to 18 mm in diameter at a maximum rotation speed of 3,000 rpm.

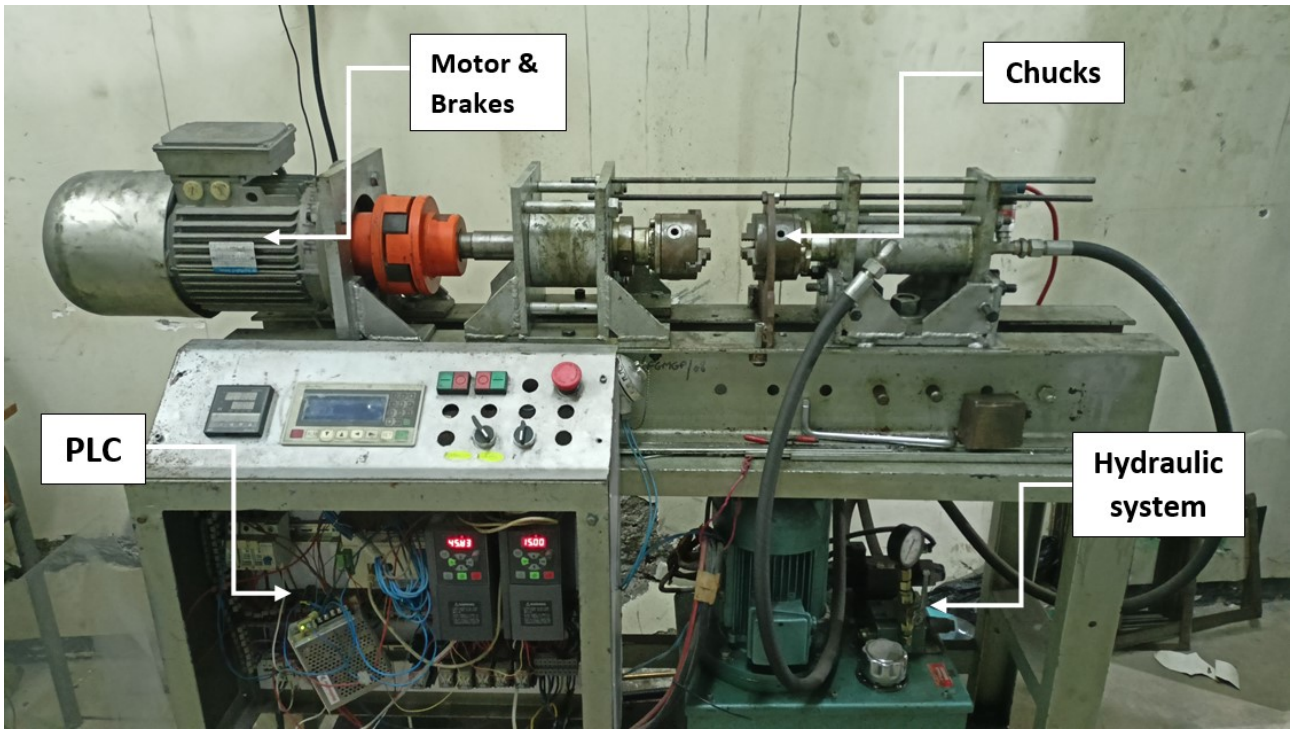

Figure 4.3: Components of the RFW machine used

4.3.2 Choice of parameters and levels

Based on the studies by Jabbar Hassan et al. [19, 33] and Paventhan et al. [18] on the rotary friction welding of AISI 304, we concluded that the friction phase of welding significantly influences the mechanical properties and microstructure of the material. Therefore, in our experiment, we chose to vary the friction time and friction pressure parameters, as well as the rotation speed, which is a critical aspect of this stage. The forging time and forging pressure were maintained constant at 6 seconds and 270 MPa throughout all the experiments.

In order to identify the right parameter levels for the experiment, we carried out a series of exploratory welds (trial and error) within the machine's operational range and backed by the findings of the previously mentioned research.

Initial parameter levels selection included friction pressures of 150 MPa and 250 MPa, friction times of 6 and 10 seconds, and rotation speeds of 2000 and 3000 rpm. Some combinations, particularly those with high friction pressure and low rotation speeds, resulted in failed welds as shown in Figure 4.4. These failures were characterized by the immediate halt of the rotating part upon contact and a sudden error display by the machine.

Figure 4.4: Failed welding operations

After several trial and error tests, we were able to identify the most suitable parameter levels, as shown in Table 4.3. These levels enabled us to construct the design matrix for the Box Behnken experimental design for the chosen factors using Minitab statistical software, presented in Table 4.4. The welded workpieces will be labeled in accordance with the run order put forward by Minitab.

Table 4.3: Parameters and their levels

Parameter	**Notation**	**Unit**	**Factor level**		
			-1	**0**	**1**
Rotation speed	N	Rpm	2500	2750	3000
Friction pressure	P	MPa	150	175	200
Friction time	T	s	6	8	10

Table 4.4: Box Behnken design matrix

Standard order	Run order	N (Rpm)	P (MPa)	T (s)
1	13	2500	150	8
2	12	3000	150	8
3	7	2500	200	8
4	14	3000	200	8
5	4	2500	175	6
6	9	3000	175	6
7	6	2500	175	10
8	5	3000	175	10
9	11	2750	150	6
10	10	2750	200	6
11	3	2750	150	10
12	1	2750	200	10
13	15	2750	175	8
14	8	2750	175	8
15	2	2750	175	8

4.3.3 Welding procedure

Following the design of the experiments using the Box Behnken design, the next step is the welding process. Once the workpieces are inserted and secured inside the chucks, we introduce the value of each parameter through the operator control panel, as illustrated in Figure 4.5.

Figure 4.5: The operator control panel

With the parameters set, we proceed to the actual welding process. The motor starts turning the rotating part, and axial pressure is applied, initiating the friction phase when the workpieces come into contact. At this moment, the temperature begins to rise, and the beading starts to form, as illustrated in Figure 4.6.

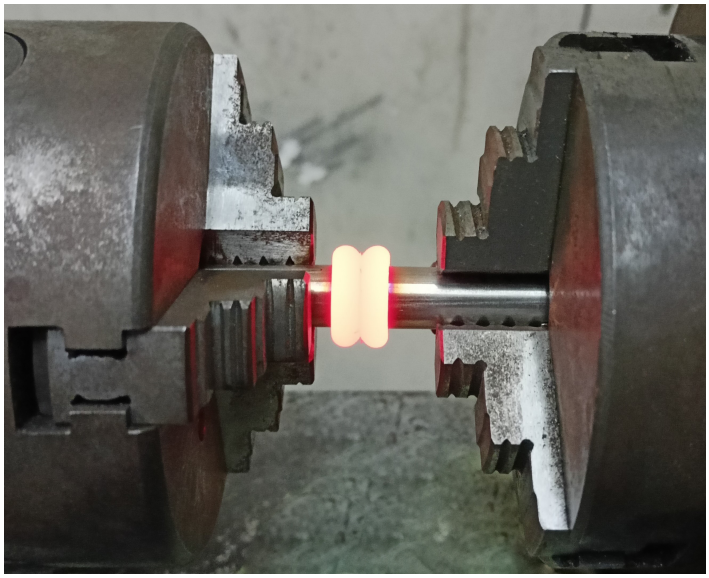

Figure 4.6: Beading formation during welding

As the beading forms, the length of the workpieces decreases, a phenomenon illustrated in Figure 4.7. This occurrence, known as the burn-off length, varies depending on the welding parameters utilized.

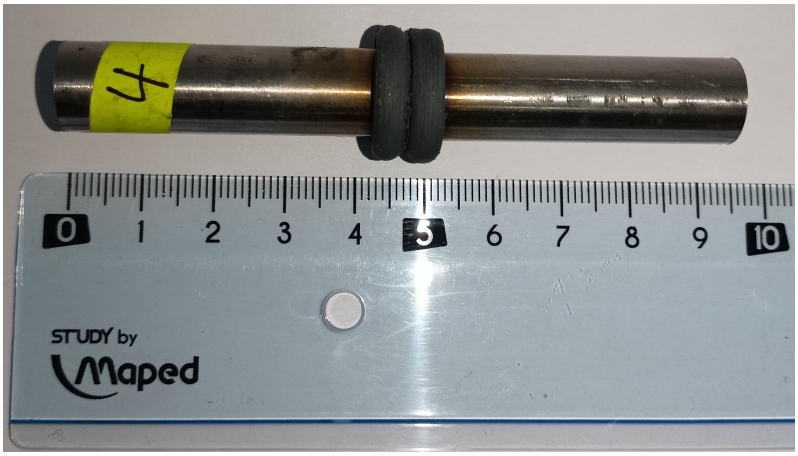

Figure 4.7: Decrease in the length of the workpieces

The final welded workpieces, showcasing the results of the rotary friction welding process, are displayed in Figure 4.8.

Figure 4.8: The welded workpieces

4.4 Mechanical tests

4.4.1 Tensile strength test

4.4.1.1 Specimens preparation

In this study, we selected the ultimate tensile strength of the joints as a key response variable for our experimental design. This choice was driven by the need to assess the mechanical integrity and performance of the joints under tensile loading conditions.

The tensile test specimens were machined from the welded workpieces shown in Figure 4.8, according to the specifications detailed in the ASTM A370-23 standard. The technical drawing of the specimen, illustrating the exact dimensions and tolerances, is provided in Appendix A.

The specimens were precisely cut and machined to the required dimensions using a Leadwell T8 CNC lathe machine (Figure 4.9) at the ACMP usinage de précision, located in Ouled Moussa, Algiers. The machining parameters used were a rotational speed of 500 Rpm and a feed rate of 0.12 mm/rev.

Figure 4.9: Leadwell T8 CNC lathe machine

The final machined tensile test specimens are displayed in Figure 4.10. Each specimen was measured with a digital caliper to verify adherence to the dimensions specified in the ASTM A370-23 standard.

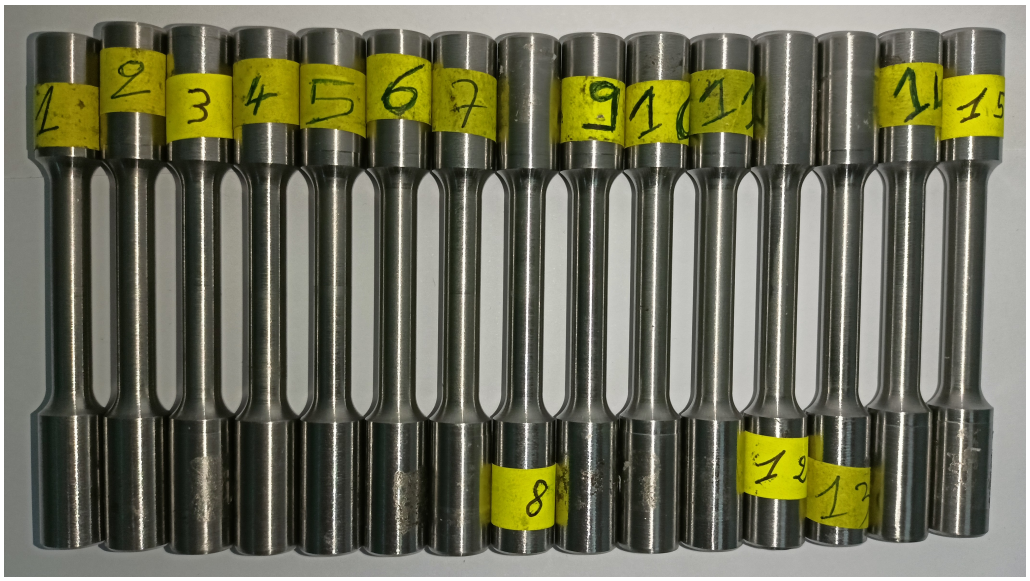

Figure 4.10: The machined tensile test specimens

4.4.1.2 Testing

The tensile strength tests were conducted at the Mechanical Engineering Department of the National Polytechnic School using a UnitedTest 100KN Electromechanical testing machine shown in Figure 4.11. Each specimen was mounted on the chucks with proper alignment taken into consideration to avoid any eccentric loading.

The tests were done at a constant displacement rate of 2mm/min as the load and elongation data were continuously recorded until the specimen fractured. The ultimate tensile strength (UTS), yield strength, and elongation at break were determined from the recorded data.

Figure 4.11: UnitedTest 100KN Electromechanical testing machine

4.4.2 Vickers hardness test

4.4.2.1 Specimen preparation

The Vickers hardness test was performed to investigate the hardness through different zones of the rotary friction welding joint. This test provides insights into the variations in hardness across the weld zone, the heat affected zone (HAZ), and the base material. A specific workpiece was welded for this purpose with the following parameters: a rotational speed of 3000 RPM, a friction pressure of 200 MPa, and a friction time of 10 seconds.

The specimen for the test was cut from the welded joint of the workpiece using a precision saw, that with careful lubrication to prevent excessive temperatures that could affect the material's hardness. The specimen was then mounted in a thermosetting resin and then polished to ensure a smooth and consistent surface finish, which is crucial for accurate hardness measurements.

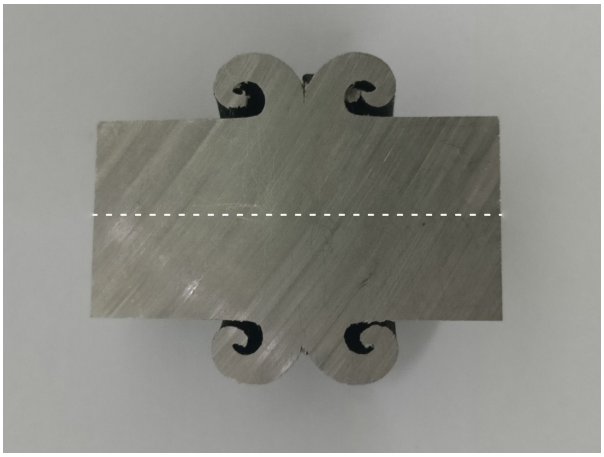

Figure 4.12: The Vickers hardness test specimen

4.4.2.2 Testing

The Vickers hardness test was conducted at the Research Center in Industrial Technologies (CRTI) using a universal hardness tester INNOVATEST NEMESIS 9000 shown in Figure 4.13, with a diamond indenter placed between two microscope lenses.

The specimen was securely placed on the stage of the universal hardness tester and the diamond indenter was pressed into the surface of the specimen with a force of 10 kgf, held for a period of 10 seconds. Indentations were made along the centerline of the specimen (apparent in Figure 4.12) at various locations across the weld zone, heat affected zone, and base material, with a step of 0.5 mm between each indentation. The Vickers hardness number (HV) was automatically determined by the hardness testing machine using the applied load and the indentation measurements.

Figure 4.13: Universal hardness tester Innovatest Nemesis 9000

4.5 Metallography analysis

4.5.1 Optical microscopy

Optical microscopy was employed to observe the microstructural features of the rotary friction welded joints. This analysis aimed to investigate the microstructure in different zones of the joint, including the weld zone, heat-affected zone (HAZ), and base material. Understanding these microstructural characteristics is essential for correlating the mechanical properties and performance of the welded joints. A specific workpiece was welded for this purpose with the following parameters: a rotational speed of 3000 RPM, a friction pressure of 200 MPa, and a friction time of 10 seconds. The specimen for optical microscopy was prepared following standard metallographic procedures to ensure high quality and reliable observations.

4.5.1.1 Specimen preparation

The welded joint was sectioned transversely to include the weld zone, HAZ, and base material. This was done using a precision saw with careful lubrication to avoid excessive heating and deformation. The sectioned specimen was then mounted in thermosetting resin to facilitate handling and to protect the edges during polishing.

The mounted specimen was sequentially polished with a mechanical polisher machine Struers LaboPol-25 using silicon carbide abrasive papers of increasing fineness, starting from 80 grit and progressing to 2400 grit, followed by polishing with aluminium oxide powder to achieve a mirror-like finish. This stepwise increase in fineness ensures that surface scratches and deformations are minimized, providing a smooth surface for microscopic analysis.

Figure 4.13: Mechanical polisher machine Struers LaboPol-25

The polished specimen was then etched using a suitable etchant for AISI 304 stainless steel to reveal the microstructural features. The etchant used was a solution of 10 grams of oxalic acid in 100 ml of distilled water (Figure 4.14a). This solution was applied electrolytically for 1 minute at 10.5 volts using PRESI POLISEC-C25 electrolytic etching machine (Figure 4.14b). This etchant effectively reveals the grain boundaries and microstructural details of AISI 304 stainless steel.

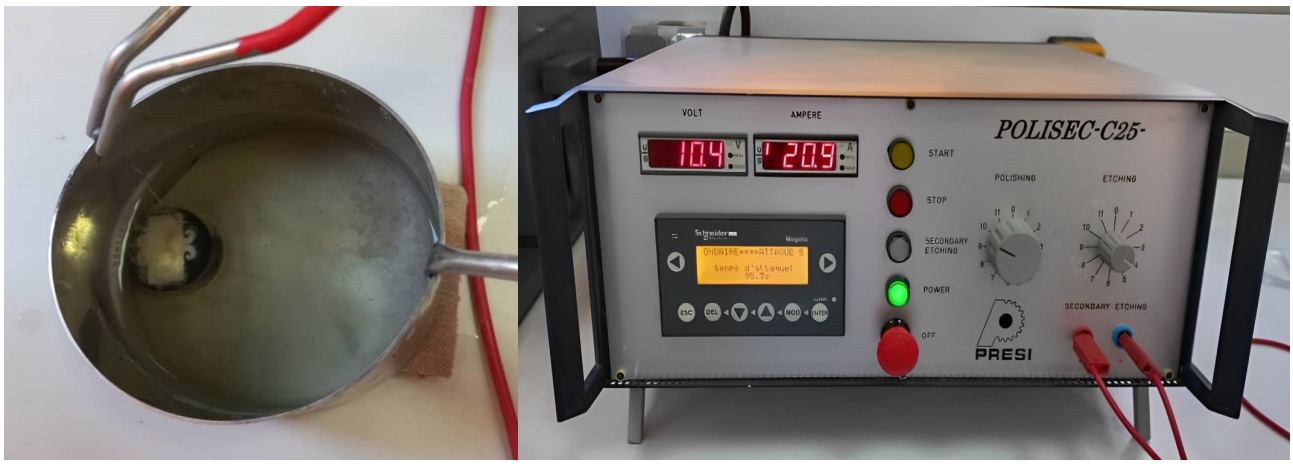

(a) Microscopy specimen in oxalic acid (b) PRESI POLISEC-C25 electrolytic etching machine

Figure 4.14: Components of the etching procedure

4.5.1.2 Microscopy observation

The microstructural examination was carried out at the Research Center in Industrial Technologies (CRTI) using a NIKON Eclipse LV100ND optical microscope.

Different magnifications were used to capture both the overall structure and fine details of the microstructure. High resolution images were also captured at various locations across the weld zone, HAZ, and base material. Key microstructural features such as grain size, phase distribution, and the presence of defects were identified and documented.

Figure 4.15: NIKON Eclipse LV100ND optical microscope and associated computer

4.5.2 Scanning electron microscopy

Scanning Electron Microscopy (SEM) was employed to observe the fracture surfaces and mode of failure of the ruptured tensile specimens from both the base metal and the welded joints. For this purpose, a specific workpiece was welded with the following parameters: a rotational speed of 3000 RPM, a friction pressure of 250 MPa, and a friction time of 8 seconds.

This analysis aimed to provide detailed insights into the fracture mechanisms and to compare the microstructural characteristics at the fracture surfaces. Understanding these characteristics helps to elucidate the failure modes and mechanical performance of the materials under tensile loading.

4.5.2.1 Specimens preparation

The specimens for SEM observation were prepared to ensure clear and detailed imaging of the fracture surfaces. After the tensile tests, the fractured specimens were carefully sectioned to obtain the fracture surfaces. This was done using a precision saw with careful lubrication to avoid introducing additional stresses. The fracture surfaces were then cleaned to remove any debris or contaminants that could interfere with the SEM imaging. The cleaned specimens were subsequently mounted on the SEM stubs for proper imaging.

4.5.2.2 Microscopy observation

The SEM analysis was conducted at the Research Center in Industrial Technologies (CRTI) using a Zeiss Gemini 300 scanning electron microscope shown in Figure 4.16.

The SEM was operated at an accelerating voltage of 20 kV, with a working distance of 11.5 to 12 mm to achieve optimal resolution and depth of field. Various magnifications were used to capture both the overall morphology and fine details of the fracture surfaces.
High-resolution images were then captured at different locations on the fracture surfaces, these will be employed to further understand the fracture mechanisms and behaviour of the base metal and the welded specimen.

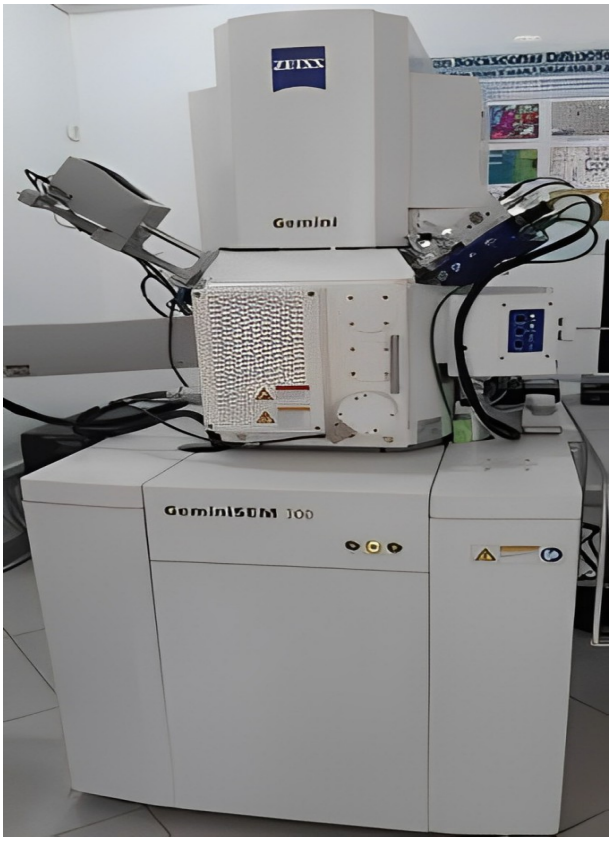

Figure 4.16: Zeiss Gemini 300 Scanning electron microscope

Chapter 5

Results and interpretations

5.1 Introduction

The purpose of this chapter is to present and interpret the results obtained from the various experimental investigations conducted throughout this study. This chapter encompasses the findings from mechanical testing, including tensile strength tests and Vickers hardness measurements, microstructural analyses performed using optical microscopy and scanning electron microscopy, as well as visual analysis of the welded joints and optimization of welding parameters. Each section provides detailed observations and discussions on the behavior and properties of the base material and welded joints, with the aim of elucidating the effects of the rotary friction welding process on the mechanical performance and microstructural characteristics.

5.2 Visual analysis of the welded joints

Visual analysis was conducted to evaluate the surface quality and integrity of the welded joints. This analysis focused on identifying surface defects, beading size, and burn-off length, which are critical indicators of the welding process's effectiveness and the resulting joint quality.

All the beadings observed in Figure 5.1 are symmetrical, which is expected given that the welding was performed between homogeneous materials. Additionally, the inspection of the welded workpieces reveals that there are no significant surface defects, indicating that the welds are of good quality. This suggests that the chosen welding parameters were effective in producing consistent and reliable welds.

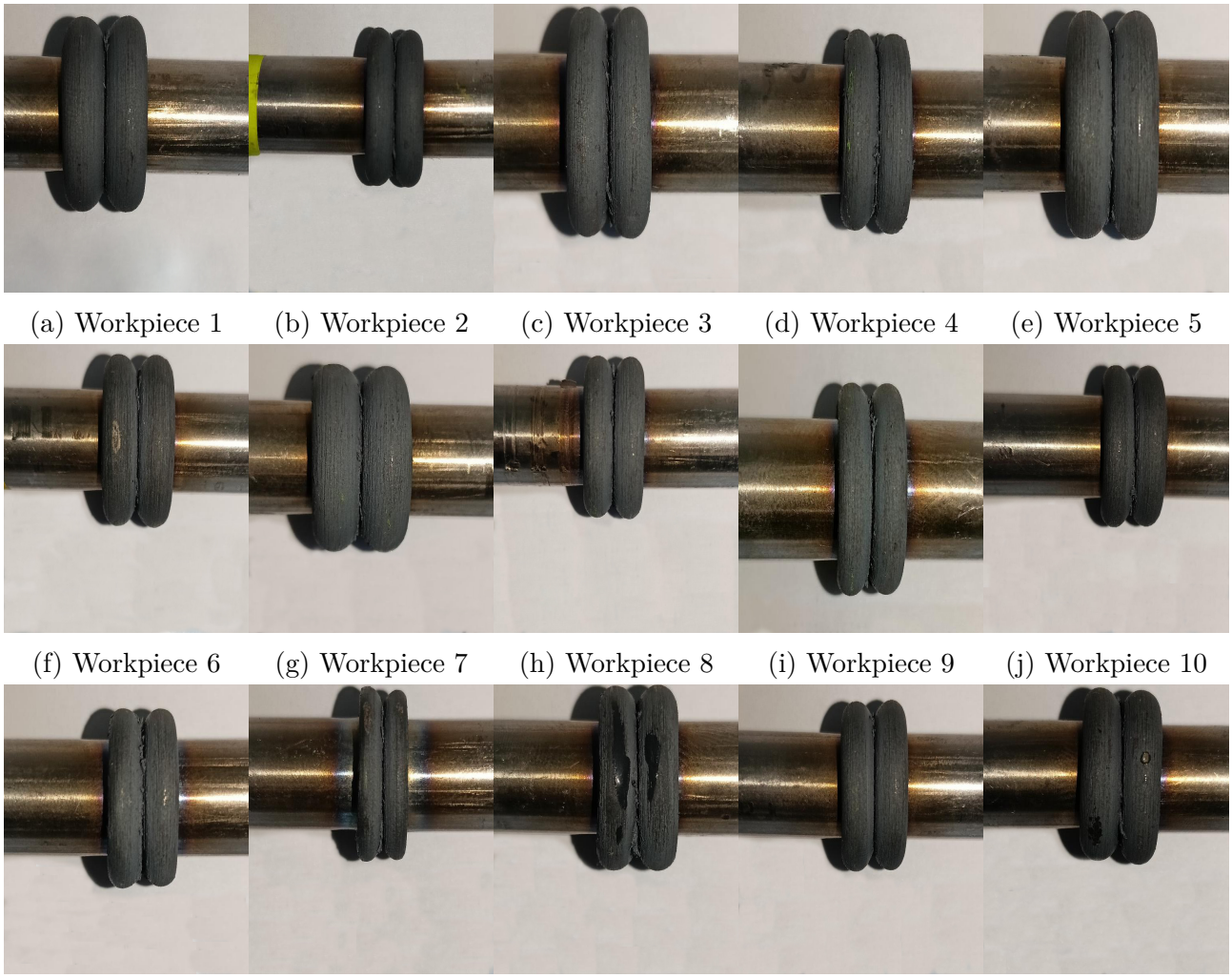

(a) Workpiece 1 (b) Workpiece 2 (c) Workpiece 3 (d) Workpiece 4 (e) Workpiece 5

(f) Workpiece 6 (g) Workpiece 7 (h) Workpiece 8 (i) Workpiece 9 (j) Workpiece 10

(k) Workpiece 11 (l) Workpiece 12 (m) Workpiece 13 (n) Workpiece 14 (o) Workpiece 15

Figure 5.1: Close up images on the beading of each workpiece

Table 5.1 and Figure 5.1 provide valuable insights into how different welding parameters affect the welding process, particularly in terms of burn-off length and beading size.
It is clear that the burn-off length and beading size are directly correlated as the burn-off length reflects the amount of material that has been displaced during the welding process and the beading represents the displaced material.

These weld characteristics vary with the variation of the different welding parameters, workpieces such as 1, 5, 6, and 7 (Figure 5.1a, 5.1e, 5.1f, and 5.1g respectively), which were subjected to moderate friction pressures combined with moderate to long friction times, show the biggest burn-off lengths together with the biggest beading sizes, as longer friction times with enough friction pressure enhance heat generation and material plasticity which allows more material displacement.

On the other hand, workpieces such as 4, 9, 11, and 12 (Figure 5.1d, 5.1i, 5.1k, and 5.1l respectively), which were subjected to moderate to low friction pressures with moderate to short friction times, show the smallest burn off lengths accompanied with the smallest beading sizes as shorter friction times with not enough pressure don't allow for sufficient heat generation and material plasticity that enable material displacement.

Table 5.1: Burn-off lengths of the workpieces

Workpiece	N (Rpm)	P (MPa)	T (s)	Burn-off length (mm)
1	2750	200	10	15.53
2	2750	175	8	11.19
3	2750	150	10	11.78
4	2500	175	6	8.71
5	3000	175	10	13.84
6	2500	175	10	14.69
7	2500	200	8	13.04
8	2750	175	8	10.40
9	3000	175	6	6.78
10	2750	200	6	10.15
11	2750	150	6	7.31
12	3000	150	8	5.26
13	2500	150	8	10.90
14	3000	200	8	11.16
15	2750	175	8	10.70

5.3 Tensile tests analysis

Figure 5.2 displays the fractured specimens after the tensile tests, illustrating the varying degrees of deformation and failure characteristics observed during the experiments.

The specimens at the top and bottom display the base metal, whereas the welded specimens are arranged vertically in between. It is important to note that all failures occurred in the welding joints, indicating that the welding process produced joints weaker in mechanical performance than that of the base metal.

Figure 5.2: Left to right specimens 1 to 15, base metal 1 on top, base metal 2 on the bottom

The tensile strength test results for the specimens, along with their corresponding stress-strain curves, are presented in Table 5.2 and Figure 5.3 respectively.

Table 5.2: Results for the tensile strength test of the different specimens

Specimen	N (Rpm)	P (MPa)	T (s)	UTS (MPa)	Elongation (%)
Base metal 1	/	/	/	732	45.1
Base metal 2	/	/	/	739	46.43
1	2750	200	10	644	24.3
2	2750	175	8	643	24.27
3	2750	150	10	631	21.97
4	2500	175	6	649	29.4
5	3000	175	10	642	22.4
6	2500	175	10	645	23.83
7	2500	200	8	668	26.9
8	2750	175	8	641	23.7
9	3000	175	6	652	26.37
10	2750	200	6	666	29.67
11	2750	150	6	645	22.33
12	3000	150	8	614	21.03
13	2500	150	8	638	22.7
14	3000	200	8	646	23.33
15	2750	175	8	647	23.43

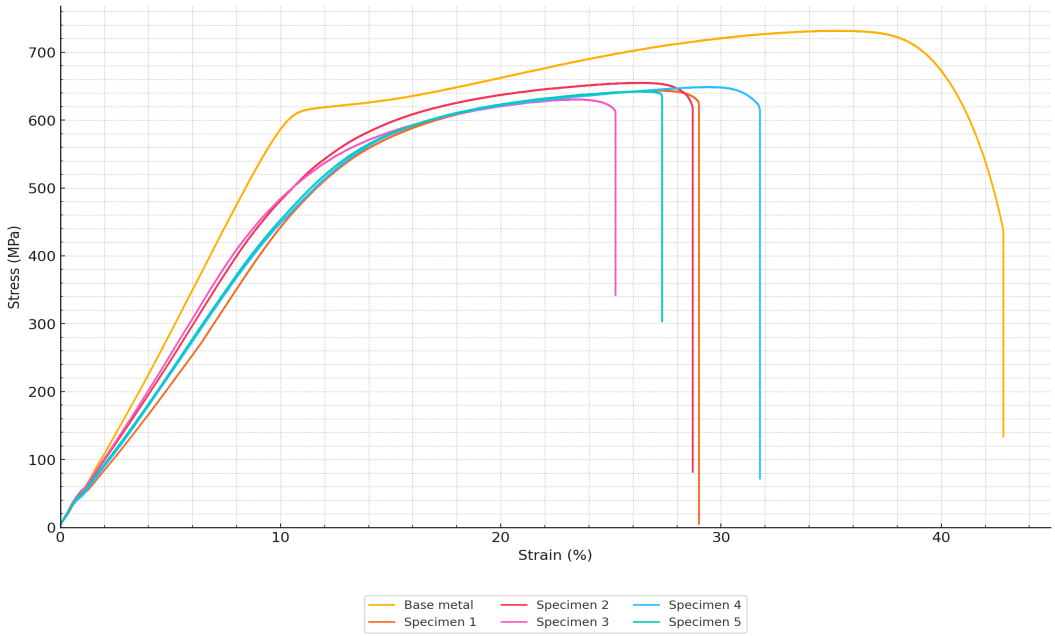

(a) Stress-strain curves of specimens 1 to 5

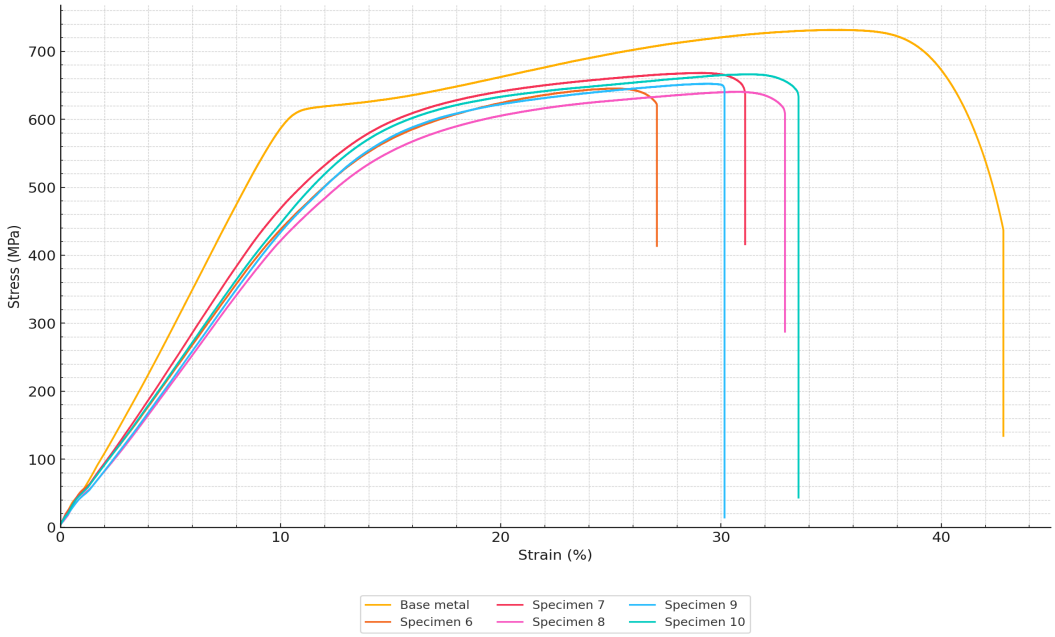

(b) Stress-strain curves of specimens 6 to 10

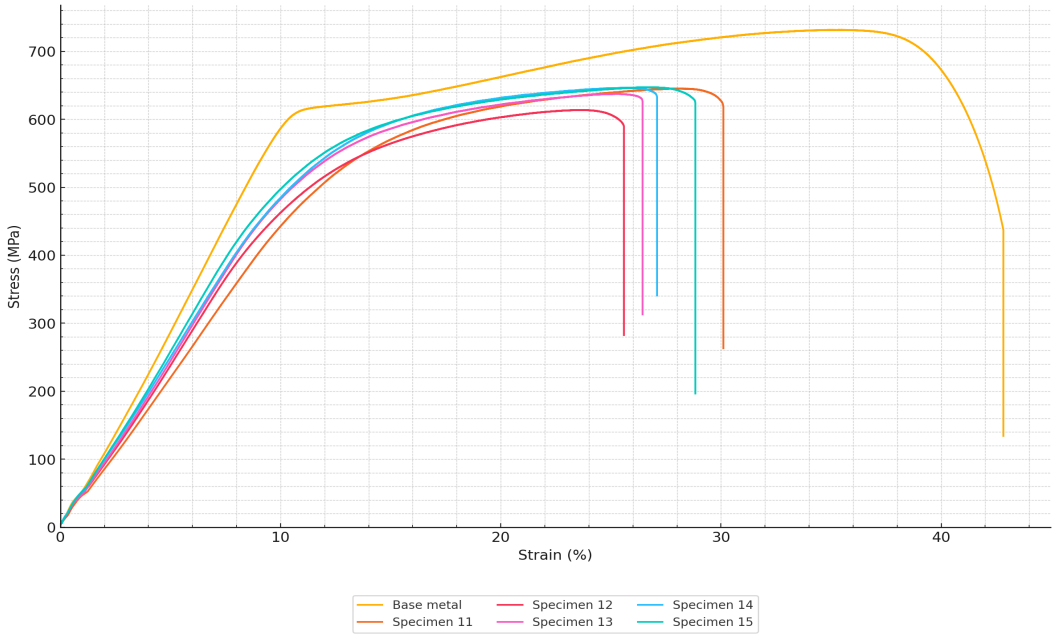

(c) Stress-strain curves of specimens 11 to 15

Figure 5.3: Stress-strain curves of the welded specimens and base metal

The first noteworthy aspect of these findings is the repeatability of both the welding procedure and the tensile strength test. The consistency of the welding process was verified using the center point specimens of the experimental design, i.e., specimens 2, 8, and 15, which demonstrated similar mechanical properties and fracture behaviors. This confirms the reliability and repeatability of the welding conditions. Additionally, the repeatability of the tensile strength test was validated by comparing the results of the base metal specimens and also by the center point specimens. The consistent results across these specimens affirm the reliability of the testing procedure.

The base metal AISI 304 stainless steel displays a typical stress-strain curve with distinct elastic and plastic regions. The elastic region is linear up to the yield point, followed by a

plastic region where the material undergoes significant permanent deformation until reaching the UTS. Beyond UTS, necking occurs, leading to eventual failure.

The stress-strain curves of the welded specimens in Figure 5.3 reveal insights into the effects of welding parameters on their mechanical properties across both the elastic and plastic regions.

All specimens demonstrate a clear elastic region where the material deforms linearly with applied stress. The elastic modulus remains largely consistent across all specimens, indicating that the initial stiffness of the material is not significantly affected by the welding process. Beyond the yield point, the plastic region shows permanent deformation, the welded specimens exhibit a plastic region moderately different than that of the base metal, indicating that the welding process slightly altered the ductility of the material. This can be observed through a decrease in both the length of the plastic region and the UTS.

The welding parameters show a significant impact on the mechanical properties of the welded joints. Specimens such as 7, 9, and 10, which were subjected to combinations of high friction pressure and rotation speed, demonstrate higher UTS and superior ductility. Conversely, specimens like 3, 12, and 13, which experienced combinations of low friction pressure and rotation speed, exhibit weaker joints with lower UTS and reduced ductility. This can be attributed to the fact that higher friction pressures and rotation speeds increase heat generation and plastic deformation at the interface, thereby improving bond quality and the overall strength of the welded joints. Preliminary observations of the results don't show a clear influence of the friction time parameter, this will be further investigated in the parameters' optimization section.

5.4 Optimization of welding parameters

5.4.1 Model optimization

Minitab statistical software was employed to design the experiments and then to model the relationship between the welding parameters and the UTS. The collected data from the tensile tests were input into the software and then, initially, a full quadratic model was used for modeling, represented by Equation 5.1 with uncoded units.

$$\begin{aligned} UTS = 465 + 0.09N + 1.33P - 4.5T - 0.000013N^2 - 0.00213P^2 + 1.04T^2 \\ +0.00008NP - 0.003NT - 0.04PT \end{aligned} \tag{5.1}$$

Where UTS is in MPa while N, P, and T are in Rpm, MPa, and seconds respectively.

Analysis of variance was conducted to evaluate the significance of the full quadratic model and its constituent terms, the findings of this analysis are displayed in the model summary in Table 5.3 and in the ANOVA table in Table 5.4.

Table 5.3: Full quadratic model summary

Metric	Value
R^2	80.59 %
R^2_{adj}	45.64 %

Table 5.4: ANOVA table of the full quadratic model

Source	DF	Adj SS	Adj MS	F-Value	P-Value
Model	9	1833.27	203.70	2.31	0.185
Linear	3	1729.00	576.33	6.52	0.035
N	1	264.50	264.50	2.99	0.144
P	1	1152.00	1152.00	13.04	0.015
T	1	312.50	312.50	3.54	0.119
Square	3	78.27	26.09	0.30	0.828
N^2	1	2.56	2.56	0.03	0.871
P^2	1	6.56	6.56	0.07	0.796
T^2	1	64.10	64.10	0.73	0.433
2-Way Interaction	3	26.00	8.67	0.10	0.958
N.P	1	1.00	1.00	0.01	0.919
N.T	1	9.00	9.00	0.10	0.762
P.T	1	16.00	16.00	0.18	0.688
Error	5	441.67	88.33		
Lack-of-Fit	3	423.00	141.00	15.11	0.063
Pure Error	2	18.67	9.33		
Total	14	2274.93			

The initial full quadratic model yielded a coefficient of determination R^2 value of 80.59%, indicating that the model explains a significant portion of the variability in the UTS response. However, the adjusted coefficient of determination R^2_{adj} value of 45.64% suggests that the model may include unnecessary terms, which do not contribute meaningfully to the prediction of the UTS.

The ANOVA results show that the overall model is not statistically significant, with a p-value of 0.185. Among the individual terms, friction pressure is the only factor that significantly influences the UTS response with a p-value of 0.015. The other linear terms of rotation speed and friction time, along with their interactions and quadratic terms, do not show a significant effect, as indicated by their high p-values.

The lack of statistical significance in the majority of the model terms implies that the full quadratic model includes terms that are not necessary for accurately predicting the UTS. This is confirmed by the low R^2_{adj} value, indicating that the model's complexity does not correspond to an improved fit.

To improve the model's accuracy and simplicity, only the most influential terms were identified and retained, i.e., the linear terms of rotation speed, friction pressure, and friction time, along with the quadratic term of friction time. The regression equation of this model is displayed in Equation 5.2, while the model summary and ANOVA table are represented in Table 5.5 and Table 5.6 respectively.

$$UTS = 715.8 - 0.023N + 0.48P - 20.4T + 1.08T^2 \tag{5.2}$$

Table 5.5: Improved model summary

Metric	Value
R^2	79.07 %
R^2_{adj}	70.69 %

Table 5.6: ANOVA table of the improved model

Source	DF	Adj SS	Adj MS	F-Value	P-Value
Model	4	1798.72	449.68	9.44	0.002
Linear	3	1729.09	576.33	12.10	0.001
N	1	264.50	264.50	5.55	0.040
P	1	1152.00	1152.00	24.19	0.001
T	1	312.50	312.50	6.56	0.028
Square	1	69.72	69.72	1.46	0.254
T^2	1	69.72	69.72	1.46	0.254
Error	10	476.21	47.62		
Lack-of-Fit	8	457.55	57.19	6.13	0.148
Pure Error	2	18.67	9.33		
Total	14	2274.93			

The refined model yielded an R^2 value of 79.07%, indicating that it still explains a substantial portion of the variability in the UTS response. The R^2_{adj} value of 70.69% demonstrates an improved fit compared to the initial model, confirming that the exclusion of insignificant terms resulted in a more accurate and reliable model.

The ANOVA results indicate that the overall model is statistically significant with a p-value of 0.002. Among the individual terms, rotation speed, friction pressure, and friction time are all statistically significant, as evidenced by their respective p-values. This signifies that these parameters have a substantial impact on UTS. The quadratic term for friction time, however, was not statistically significant, suggesting that the effect of friction time on UTS is primarily linear.

To further deepen the analysis, the residuals vs fitted values plot in Figure 5.4 was examined. This plot is a crucial diagnostic tool that helps assess the goodness of fit for the regression model by displaying the residuals (the differences between observed and predicted UTS values) against the fitted values (the predicted UTS values from the model).

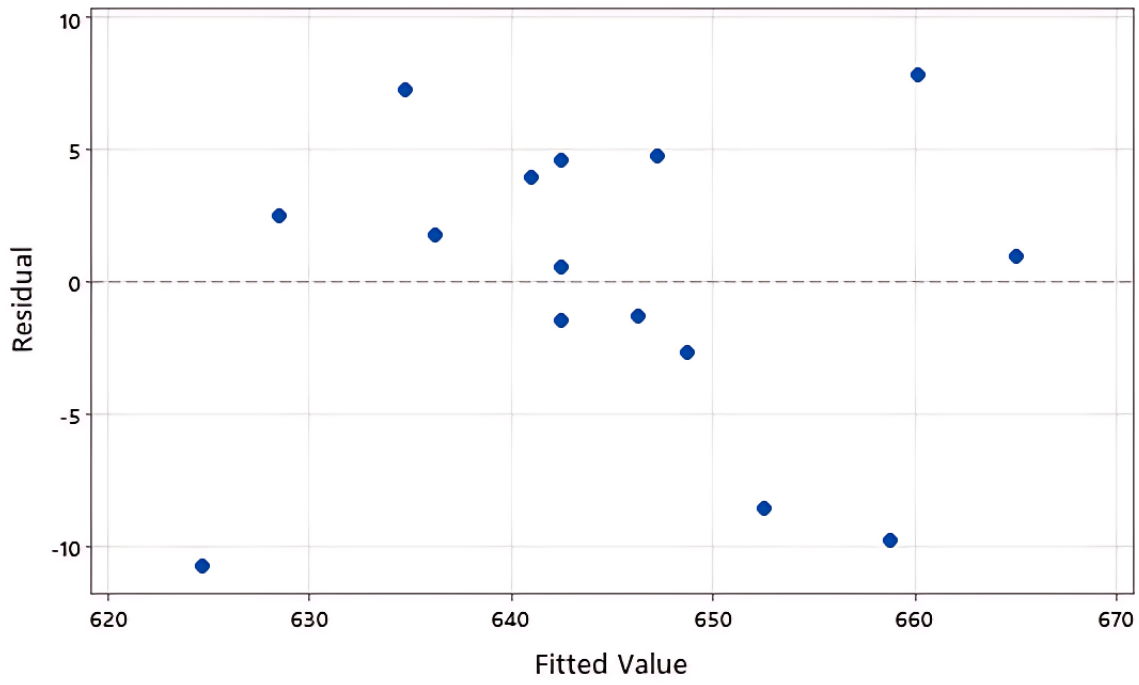

Figure 5.4: Residuals Vs Fitted values scatter plot

Upon examining the plot, it becomes apparent that the residuals are randomly scattered around the horizontal axis (residual = 0). This random distribution suggests that the model does not exhibit obvious patterns of systematic errors, indicating that the assumptions about the relationship between the predictors and the response variable are reasonably accurate.

The absence of a clear pattern among the residuals suggests that the model is appropriate for this dataset. If the residuals had exhibited an apparent pattern, such as a curved shape, it might have indicated that another relationship exists between the predictors and the response variable, one that is not present in the actual model, necessitating a different modeling approach.

While the overall pattern of residuals is encouraging, a few points stand out as outliers. Specifically, there are residuals further from the horizontal axis at fitted values around 620 and 660. These outliers are likely due to experimental errors, which can arise from various sources such as inaccuracies in welding and testing procedures. Identifying, understanding and correcting these errors is crucial for ensuring the robustness of models of future experiments.

Since the residual analysis indicated that the model is reasonably accurate and does not exhibit systematic errors, we can confidently proceed to optimize the welding parameters with the goal of achieving the optimal mechanical performance of the welded joints, i.e., maximizing the UTS. Using Minitab statistical software, the optimization process identified the best combination of rotation speed, friction pressure, and friction time. The contour plots and response surfaces of UTS in Figure 5.5 can help further understand this optimization process and the influence of each parameter and their interactions on the response.

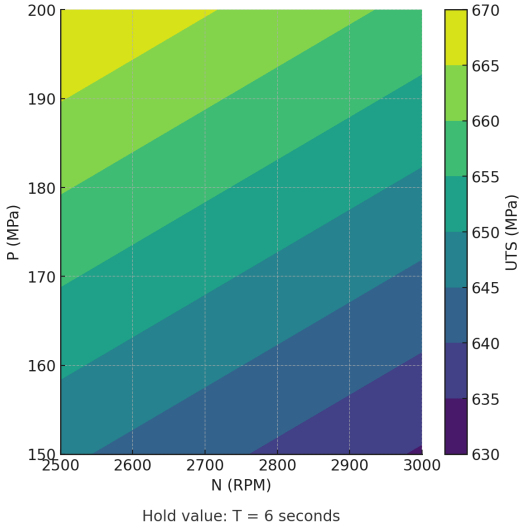

(a) P and N interaction contour plot

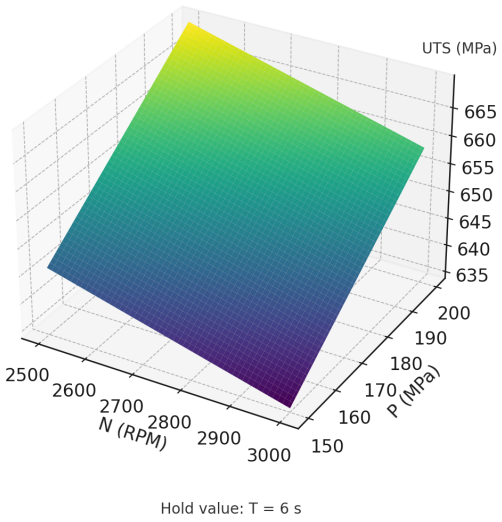

(b) P and N interaction response surface

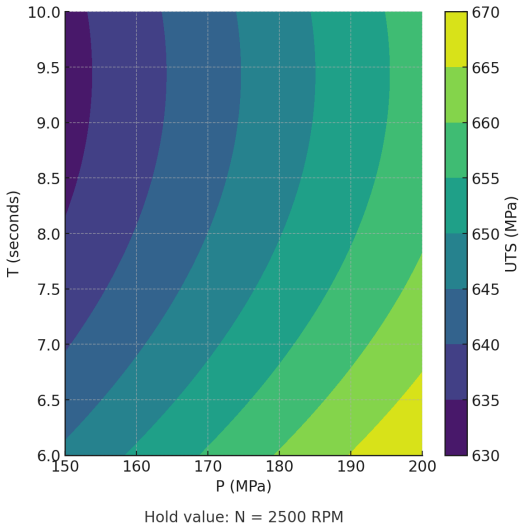

(c) P and T interaction contour plot

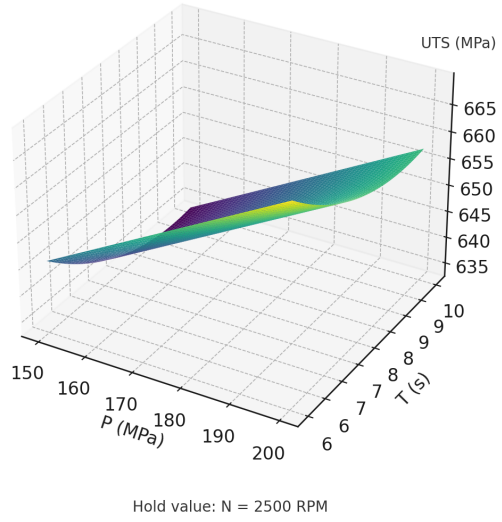

(d) P and T interaction response surface

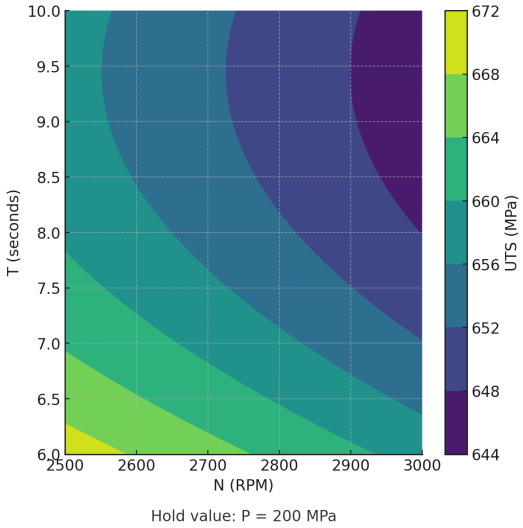

(e) T and N interaction contour plot

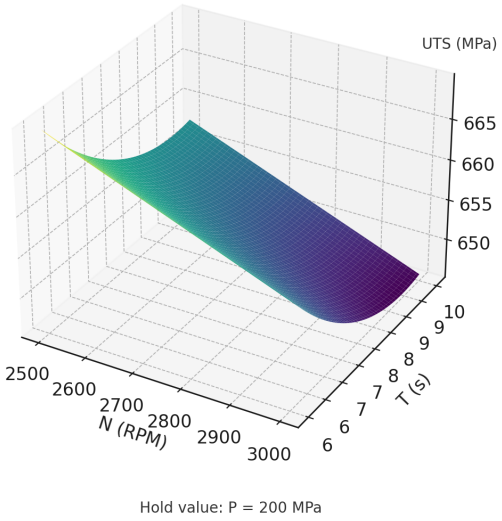

(f) T and N interaction response surface

Figure 5.5: UTS contour plots and response surfaces

The desirability graph in Figure 5.6 shows that the optimal settings for the welding parameters are a rotation speed of 2500 Rpm, a friction pressure of 200 Mpa, and a friction time of 6 seconds. These settings yield a predicted UTS of 669.98 MPa, with a desirability score of 1.000, indicating the best possible outcome based on the model.

Examining the individual parameter plots, we can see distinct relationships between each parameter and the UTS. For rotation speed, there is a negative slope, indicating that as the rotation speed increases, the UTS decreases. In contrast, the friction pressure plot shows a positive slope, indicating that as the friction pressure increases, the UTS also increases, whereas The friction time plot exhibits a non-linear relationship with UTS, showing a peak at the optimal point.

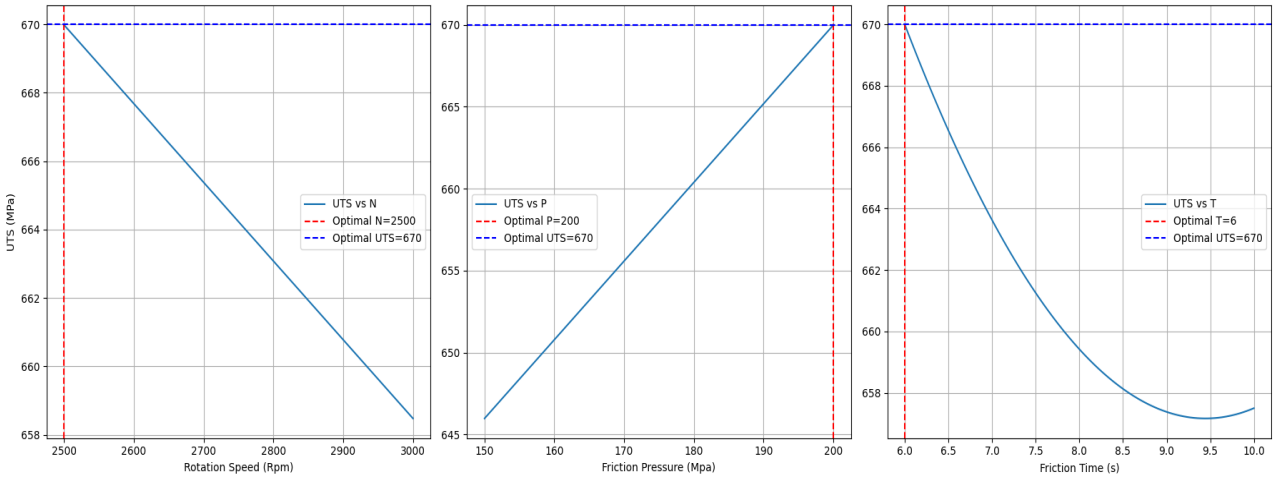

Figure 5.6: Desirability plot of optimal parameters

These optimal parameters yield an UTS that surpasses other welding processes, such as Metal Inert Gas (MIG) welding, which has a UTS of 652 MPa [34], and Shielded Metal Arc Welding (SMAW), with an UTS of 561 MPa [35], on the same material. The UTS achieved with these optimized settings is comparable to that obtained with Tungsten Inert Gas (TIG) welding, which reaches 675 MPa [34], without the need for filler metal. This comparison highlights the effectiveness of the optimized parameters in achieving excellent mechanical performance, making this welding process highly competitive with other established welding techniques.

5.4.2 Model validation

To further validate the model, an extrapolation was performed beyond the defined parameter domains. An additional workpiece was welded with the following parameters: a rotational speed of 3000 RPM, a friction pressure of 250 MPa, and a friction time of 8 seconds.
The tensile test for this specimen was conducted, and the UTS was measured at 673 MPa, the corresponding stress-strain curve is shown in Figure 5.7.

Using the regression model in Equation 5.2, the predicted UTS for the extrapolated parameters was determined to be 671.92 MPa, approximately 672 MPa.

The comparison between the observed and predicted UTS shows a very close agreement. The difference between the observed UTS and the predicted UTS is only 1.08 MPa, with a relative error of 0.16%, indicating that the model is robust even when extrapolated beyond the original

parameter domains, as long as the welding is feasible with that parameter combination.

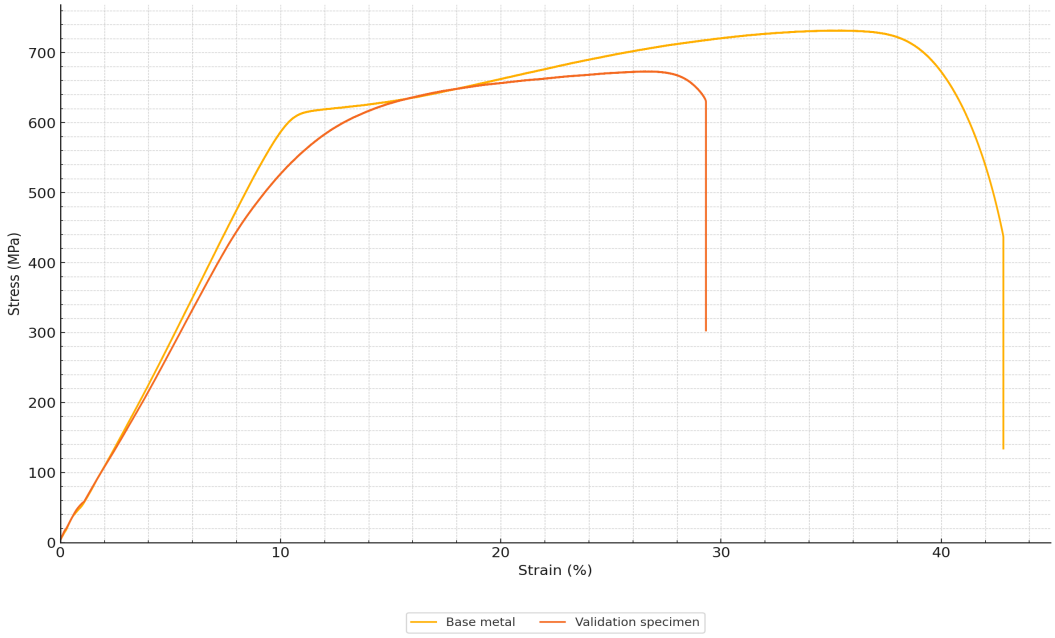

Figure 5.7: Stress-strain curve of the validation specimen

5.4.3 Tensile fracture mode analysis

SEM imaging was conducted to examine the fracture surfaces of both the base metal and the welded validation specimen. The observations from the SEM images in Figure 5.8 provide insights into the fracture behavior and the underlying microstructural characteristics that influence the mechanical properties of the materials.

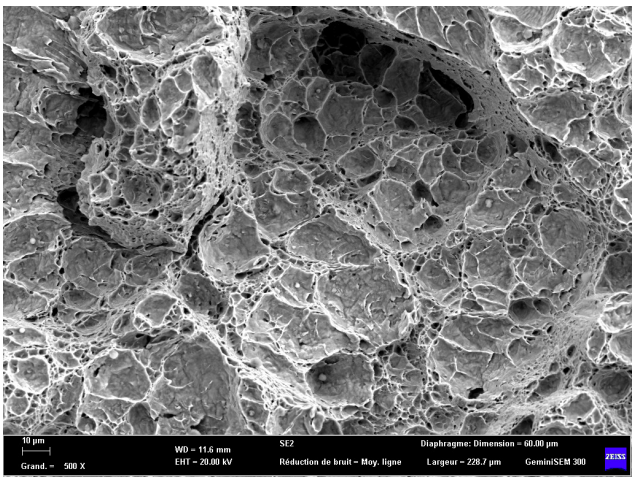

(a) Base metal with x500 magnification

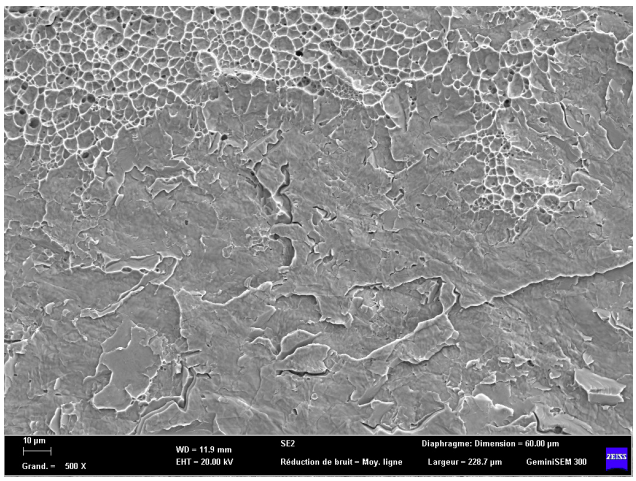

(b) Welded specimen with x500 magnification

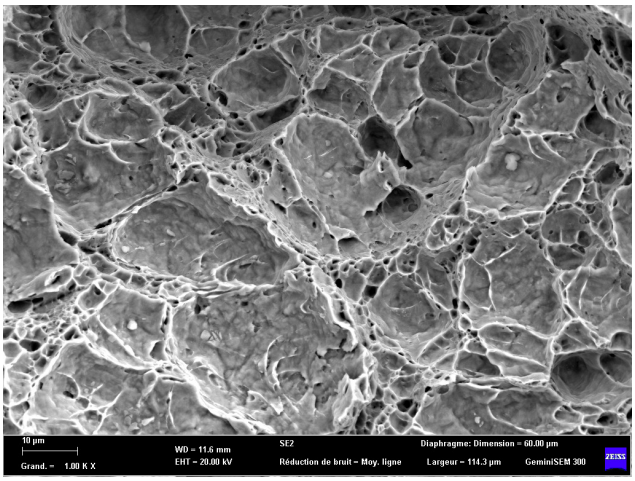

(c) Base metal with x1000 magnification

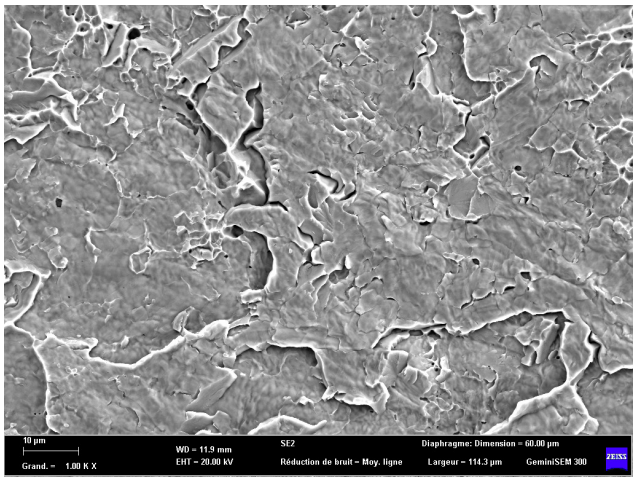

(d) Welded specimen with x1000 magnification

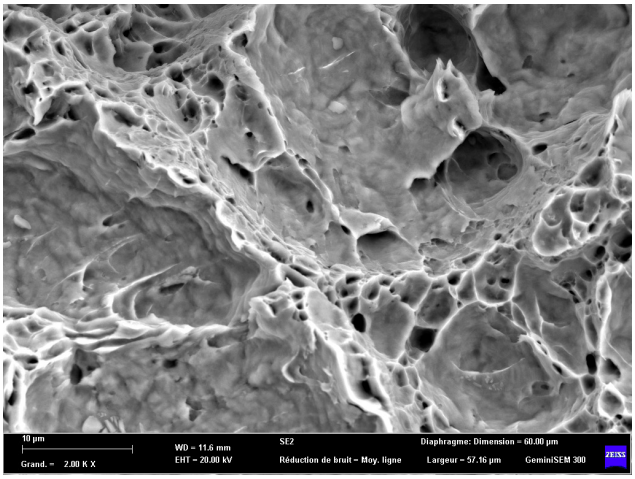

(e) Base metal with x2000 magnification

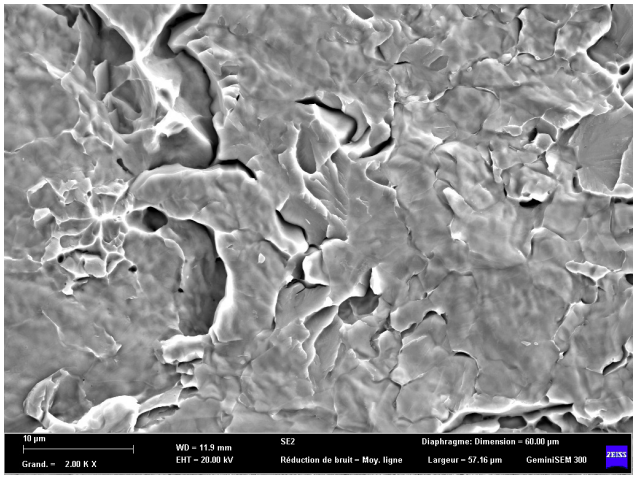

(f) Welded specimen with x2000 magnification

Figure 5.8: SEM images of the fracture surfaces of the base metal and welded specimen

The SEM images of the base metal's fracture surface reveals a typical ductile fracture morphology. The surface is covered with numerous deep dimples, indicative of significant plastic deformation before fracture. The fracture surface appears uniform, suggesting homogeneous material properties and consistent ductile behavior throughout the base metal.
This ductile fracture, along with the presence of dimples, confirms the base metal's ability to absorb a substantial amount of energy, thereby its toughness, and demonstrates its capability

of significant plastic deformation before failure.

In contrast, the SEM images of the welded specimen's fracture surface exhibits a mixed fracture behavior. The surface shows regions with ductile dimples as well as areas with cleavage planes, which are indicative of brittle fracture. This heterogeneous fracture surface reflects the varying mechanical properties within the welded joint.
The presence of both dimples and cleavage planes indicates that certain regions of the weld are more brittle, likely due to microstructural changes caused by the welding process, these brittle regions have lower toughness and are more prone to sudden fracture without significant plastic deformation. The heterogeneity in the fracture surface is typical of welded joints, where different zones exhibit distinct microstructures and mechanical properties.

To further illustrate the differences in mechanical behavior between the base metal and the welded specimen, Figure 5.9 showcases both specimens after tensile testing. The image clearly highlights the extent of plastic deformation in each specimen. The base metal exhibits a significantly greater elongation, indicative of its ductile nature, whereas the welded specimen shows less elongation, reflecting its mixed fracture behavior.

Figure 5.9: Comparison of plastic deformation between specimens. The base metal specimen is on top and the welded specimen is on the bottom

These differences showcase the effects of the welding process on material behavior, and it highlights the necessity of optimizing welding parameters to enhance weld toughness and minimize the occurrence of brittle regions, thereby improving the overall reliability of the welded joints.

5.5 Microstructural analysis

The provided microscopic images in Figure 5.10 offer a comprehensive view of the microstructure of the welding joint formed by the RFW process. In this analysis, we focus on the key microstructural features observed across the weld joint.

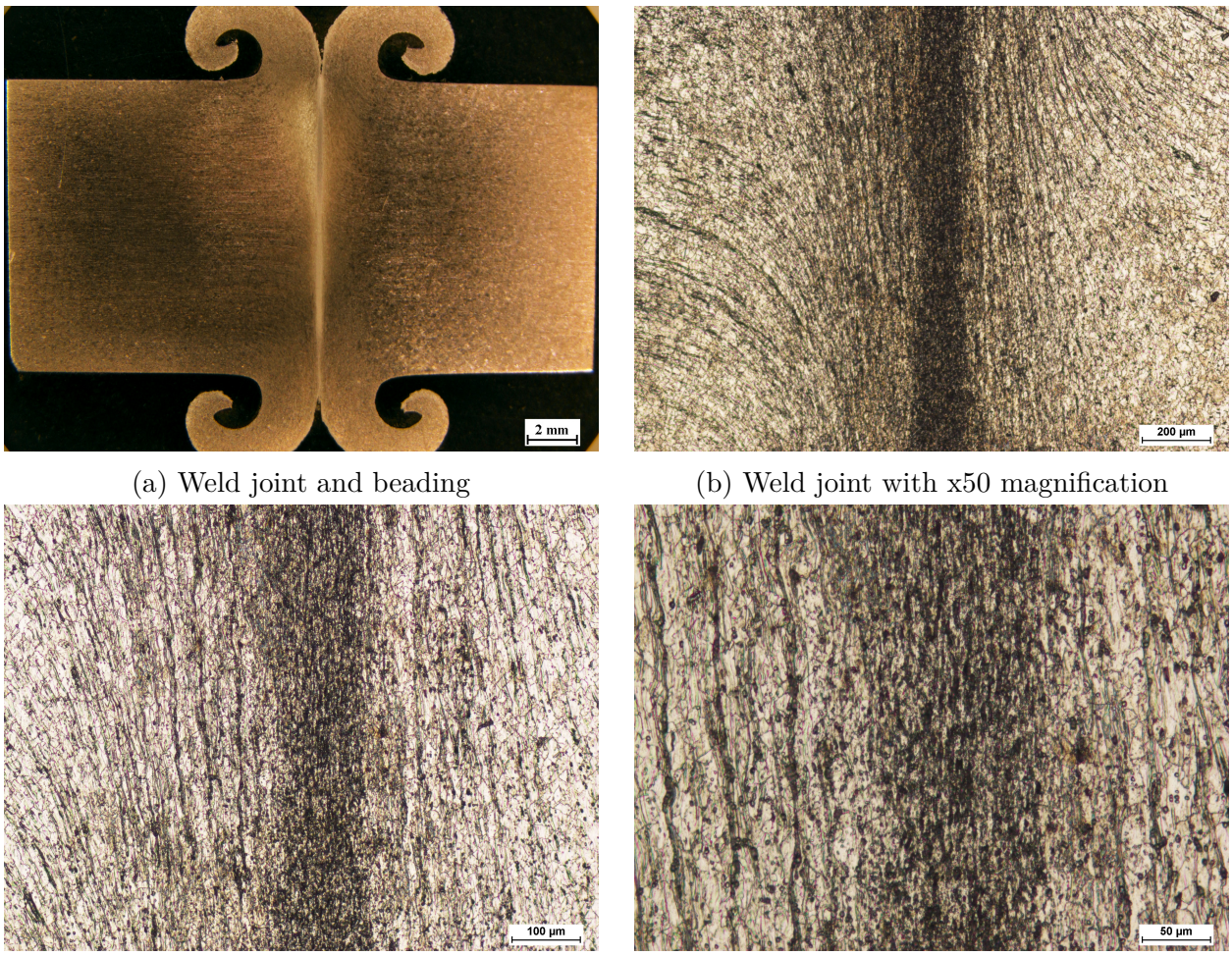

(a) Weld joint and beading

(b) Weld joint with x50 magnification

(c) Weld joint with x100 magnification

(d) Weld joint with x200 magnification

Figure 5.10: Microscopic images of the microstructure of the weld joint

The weld zone, located centrally in the images, exhibits a fine grain structure. This fine-grained microstructure is indicative of dynamic recrystallization resulting from the intense plastic deformation and heat generated during the RFW process. The rapid cooling and severe plastic deformation experienced in this zone lead to a significant grain refinement, which is crucial for enhancing the mechanical properties of the welded joint. The homogeneity of the weld zone, with minimal visible defects, underscores the effectiveness of the RFW process in producing high-quality welds.

Adjacent to the weld zone is the heat-affected zone. The HAZ shows a distinct transition in microstructure from the fine grains of the weld zone to slightly larger grains. This region experiences elevated temperatures but does not undergo the same level of plastic deformation as the weld zone. Consequently, grain coarsening is observed as one moves from the weld zone into the HAZ. This grain growth is a result of the thermal exposure during welding, which facilitates partial recrystallization and grain boundary movement. The transition between the weld zone and the HAZ is marked by a gradual increase in grain size, reflecting the thermal gradient and the extent of heat exposure.

Further from the weld center, the base metal retains its original microstructure. The grains in the base metal are relatively larger and more equiaxed compared to those in the weld zone and HAZ. This region shows minimal impact from the welding process, maintaining its original grain size and morphology. The clear distinction between the base metal and the affected

regions highlights the localized nature of the thermal and mechanical effects induced by RFW.

An important aspect of this analysis is the influence on the rotating part of the workpiece during the welding process, located on the left side of the images. The rotational motion during welding results in asymmetric frictional heat and plastic deformation. This asymmetry is reflected in the grain flow patterns and the microstructural features observed. The rotating part experiences more intense frictional heat, contributing to finer grain structures in both the weld zone and HAZ on the left side.

5.6 Hardness analysis

The Vickers hardness test results provide valuable insights into the hardness distribution across the weld zone, HAZ, and base metal. The plotted data in Figure 5.11 shows how the hardness varies as we move from one side of the weld joint to the other.

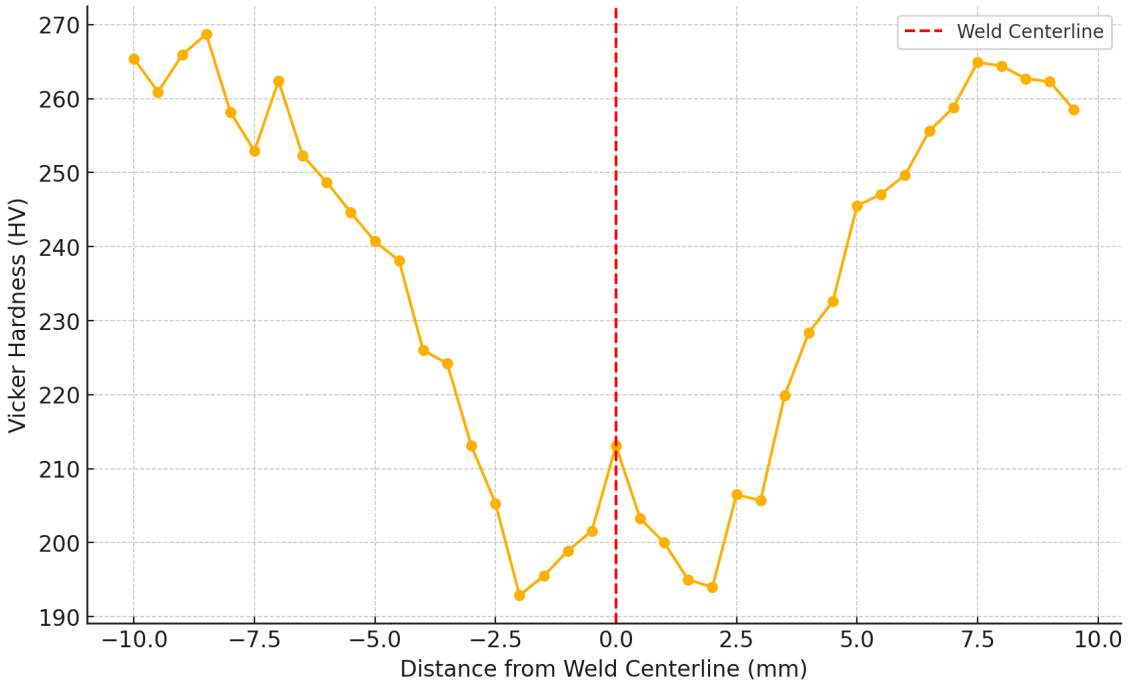

Figure 5.11: Hardness profile across the weld joint

The hardness profile indicates significant variations across the weld joint. The highest hardness values are observed at the extremities of the measured region, which correspond to the base metal areas. Here, the hardness values range around 260-270 HV, reflecting the original material properties before welding.

As we move towards the weld centerline, there is a noticeable decrease in hardness values. This decrease begins gradually and becomes more pronounced within the HAZ. The lowest hardness values are observed around the weld centerline, with a minimum of 193 HV. This reduction in hardness around the weld centerline area can be attributed to the high temperatures and the subsequent cooling rates experienced during the RFW process. This thermal cycle cause changes in the microstructure, including grain coarsening and possible tempering effects, leading to lower hardness. The weld centerline itself shows a slight recovery in hardness, which could

be due to localized effects of dynamic recrystallization and the presence of finer grain structures resulting from the intense plastic deformation and rapid cooling.

The trend of decreasing hardness values towards the centerline is symmetrical, which is expected in such a process due to the similar material, thermal, and mechanical conditions on both sides of the joint. This hardness distribution is consistent with the microstructural observations, aligning perfectly with the expected variations in grain structure and the effects of thermal and mechanical processes that occur during RFW.

5.7 Conclusion

In this chapter, we presented a detailed analysis of the experimental results obtained from the RFW of AISI 304 stainless steel. The visual inspection of the welded joints revealed uniform bead formation and minimal defects, whereas the tensile tests and the optimization of welding parameters proved effective in identifying the optimal conditions for maximizing UTS and the validation procedure confirmed the accuracy and reliability of the predictive model.

Overall, the results validate the effectiveness of RFW in producing high quality joints in AISI 304 stainless steel. The insights gained from this study provide a robust foundation for further research and industrial applications, emphasizing the importance of precise control over welding parameters to achieve desired mechanical properties.

General Conclusion

This thesis has delved into the optimization of parameters influencing rotary friction welding joints, employing the Box-Behnken design approach to achieve superior joint quality. The comprehensive investigation undertaken in this study has provided significant insights into the RFW process, its parameters, and their interactions, leading to a systematic and efficient optimization methodology.

The study successfully employed the Box-Behnken design, a response surface methodology, to systematically vary and optimize the welding parameters. This approach allowed for a comprehensive exploration of the interactions between multiple parameters, leading to the identification of the optimal conditions for the RFW process. The optimal parameters were found to be a rotational speed of 2500 Rpm, a friction pressure of 200 MPa, and a friction time of 6 seconds. Experimental results demonstrated that these optimized welding parameters significantly enhanced the mechanical properties of the welded joints, and the microstructural analysis further confirmed the quality of the welds, with minimal defects and superior metallurgical structure. The use of analysis of variance provided a robust framework for interpreting the experimental data, the models developed through this analysis were validated and found to be effective in predicting the outcomes of the welding process under various conditions.

Future research could explore the application of the Box-Behnken design to other materials and welding processes, further broadening the scope of optimization techniques in welding technology. The flexibility of the Box-Behnken design allows for the investigation of additional parameters without the loss of existing data, facilitating a more comprehensive optimization. Additionally, other response variables such as bending strength or fatigue resistance could be investigated to provide a more holistic understanding of the joint performance. Furthermore, expanding the use of simulation and modeling tools to predict welding outcomes and optimize parameters without extensive experimental trials would be a promising direction for future work. Furthermore, expanding the use of simulation and modeling tools to predict welding outcomes and optimize parameters without extensive experimental trials would be a promising direction for future work.

In conclusion, this thesis has advanced the field of rotary friction welding by optimizing key parameters to achieve high quality joints. The integration of experimental and statistical methods has proven to be an effective approach, offering practical solutions and setting the stage for future innovations in welding technology

Bibliography

[1] Roland CAZES. Soudage par friction. *Techniques de l'ingénieur Travail des matériaux - Assemblage*, (ref. article : b7745), 1996.

[2] Nisarg Shete and Swapnil Deokar. A review paper on rotary friction welding. 5:1557 – 1560, 06 2017.

[3] M. Maalekian. Friction welding – critical assessment of literature. *Science and Technology of Welding and Joining*, 12(8):738–759, 2007.

[4] CED Rowe and Wayne M Thomas. Advances in tooling materials for friction stir welding. *TWI and Cedar Metals Ltd*, pages 1–11, 2005.

[5] Nejah Jemal. *Contribution à la caractérisation thermique et mécanique de la zone soudée en FSW*. Phd thesis, Arts et Métiers ParisTech, December 2011.

[6] I. Bhamji, M. Preuss, P. L. Threadgill, and A. C. Addison. Solid state joining of metals by linear friction welding: A literature review. *Materials Science and Technology*, 27(1):2–12, 2011.

[7] Hiroshi Kuroki, Koji Nezaki, Tsukasa Wakabayashi, and Kenji Nakamura. Application of linear friction welding technique to aircraft engine parts. *IHI Eng. Rev*, 47(1):40–43, 2014.

[8] Achilles Vairis, George Papazafeiropoulos, and Andreas-Marios Tsainis. A comparison between friction stir welding, linear friction welding and rotary friction welding. *Advances in Manufacturing*, 4, 12 2016.

[9] A. Nasution, H. Gustami, S. Suprastio, M.A. Fadillah, J. Octavia, and S. Saidin. Potential use of friction welding for fabricating semi-biodegradable bone screws. *International Journal of Automotive and Mechanical Engineering*, 19, 06 2022.

[10] ir. Koen Faes. Soudage par friction. Institut Belge de la Soudure. bil-ibs.be/fr/publicatie/soudage-par-friction. Accessed: 30-03-2024.

[11] KUKA Industries. Rotary friction welding. kuka.com/fr-fr/produits-et-prestations/machines-de-fabrication/machines-de-soudage-par-friction-en-rotation. Accessed: 30-03-2024.

[12] Khalfallah Fares. *Soudage par friction de l'acier avec du céramique*. Phd thesis, Université Mohamed Khider-Biskra, March 2020.

[13] K. S. Prasad, C. Srinivasa Rao, D. Nageswara Rao. A Review on Welding of AISI 304L Austenitic Stainless Steel. *Journal for Manufacturing Science and Production*, 14(1):1–11, 2014.

[14] PS Korinko and SH Malene. Considerations for the weldability of types 304l and 316l stainless steel. *Practical failure analysis*, 1:61–68, 2001.

[15] M Kaladhar, K Venkata Subbaiah, and CH Srinivasa Rao. Machining of austenitic stainless steels–a review. *International Journal of Machining and Machinability of Materials*, 12(1-2):178–192, 2012.

[16] Harold M Cobb. The naming and numbering of stainless steels. *Iron and Steel Society*, pages 173–178, 1999.

[17] Gurunath Shinde and Prakash Dabeer. Review of experimental investigations in friction welding technique. *Sustainable Development*, 373:384, 2017.

[18] R Paventhan et al. Optimizing Friction Welding Parameters in AISI 304 Austenitic Stainless Steel and Commercial Copper Dissimilar Joints. *Coatings*, 13(2):261, 2023.

[19] A Jabbar Hassan, T Boukharouba, and D Miroud. Friction welding of AISI 304: effect of friction time on micro-structure, micro-hardness and tension-compression properties. *Acta Metallurgica Slovaca*, 26(3):78–83, 2020.

[20] Isaac Newton. Letter to Henry Oldenberg. July 6th, 1672.

[21] C. H. Lauro, R. B. D. Pereira, L. C. Brandão, and J. P. Davim. *Design of Experiments—Statistical and Artificial Intelligence Analysis for the Improvement of Machining Processes: A Review*, pages 89–107. Springer International Publishing, 2016.

[22] Jacques GOUPY. Plans d'expériences. *Techniques de l'ingénieur Conception et Production*, base documentaire : TIP083WEB.(ref. article : p230), 1997.

[23] D.C. Montgomery. *Design and Analysis of Experiments, 8th Edition*. John Wiley & Sons, Incorporated, 2012.

[24] J. Goupy and L. Creighton. *Introduction to Design of Experiments with JMP Examples*. SAS Press series. SAS Institute, 2007.

[25] Jacques GOUPY. Modélisation par les plans d'expériences. *Techniques de l'ingénieur Instrumentation et méthodes de mesure*, base documentaire : TIP676WEB.(ref. article : r275), 2016.

[26] Benjamin Durakovic. Design of experiments application, concepts, examples: State of the art. *Periodicals of Engineering and Natural Sciences*, 5:421–439, 12 2017.

[27] Robert Mee. *A Comprehensive Guide to Factorial Two-Level Experimentation*. 2009.

[28] Barbara G Tabachnick and Linda S Fidell. *Experimental designs using ANOVA*, volume 724. Thomson/Brooks/Cole Belmont, CA, 2007.

[29] Steven F Sawyer. Analysis of variance: the fundamental concepts. *Journal of Manual & Manipulative Therapy*, 17(2):27E–38E, 2009.

[30] Martin G Larson. Analysis of variance. *Circulation*, 117(1):115–121, 2008.

[31] Richard C. Sprinthall. *Basic Statistical Analysis: Pearson New International Edition*. Pearson, 9th edition, 2013.

[32] Cheryl Ann Willard. *Statistical Methods: An Introduction to Basic Statistical Concepts and Analysis*. Routledge, 2nd edition, 2020.

[33] A Jabbar Hassan, T Boukharouba, D Miroud, and S Ramtani. Metallurgical and mechanical behavior of aisi 316-aisi 304 during friction welding process. *International Journal of Engineering*, 32(2):306–312, 2019.

[34] Javed Kazi, Syed Zaid, Syed Mohd Talha, Mukri Yasir, and Dakhwe Akib. A review on various welding techniques. *International Journal of Modern Research*, 5(2):22–28, 2015.

[35] PS Gowthaman, P Muthukumaran, J Gowthaman, and C Arun. Review on mechanical characteristics of 304 stainless steel using smaw welding. *International Journal of Science and Technology*, 2(2):32–37, 2017.

APPENDIX

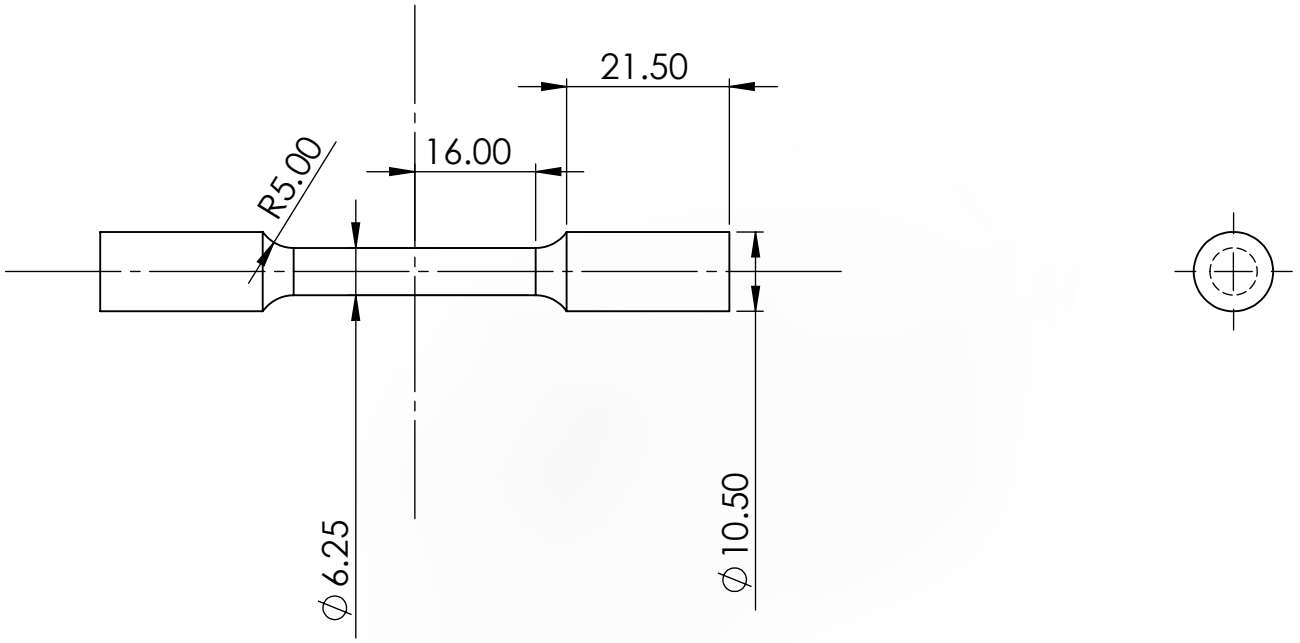

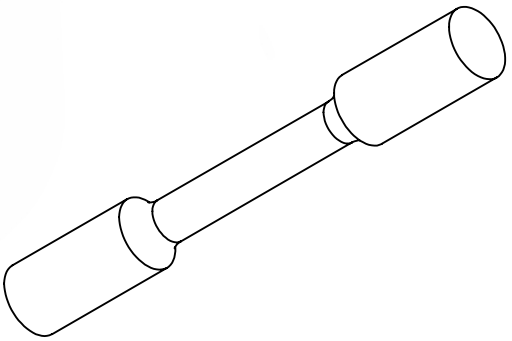

NATIONAL	POLYTECHNIC	SCHOOL
SCALE 1:1	TENSILE TEST SPECIMEN	MECHANICAL ENG DEP
STUDENT BOUTIARA		
SUPERVISOR SAIDI		
SUPERVISOR JABBAR HASSAN		
MATERIAL AISI 304		02/07/2024